

## Article

# Impact of Gaseous Pollutants Reduction on Fine Particulate Matter and Its Secondary Inorganic Aerosols in Beijing–Tianjin–Hebei Region

Zhe Wei <sup>1,2</sup>  and Norhaslinda Mohamed Tahrin <sup>1,\*</sup>

<sup>1</sup> School of Physics, Universiti Sains Malaysia, Gelugor 11800, Pulau Pinang, Malaysia; weizhe@student.usm.my

<sup>2</sup> School of Energy and Environmental Engineering, Hebei University of Engineering, Handan 056038, China

\* Correspondence: haslinda@usm.my

**Abstract:** A reduction in gaseous pollutants is an important method for mitigating PM<sub>2.5</sub> concentration in the atmosphere, and the reduction in SO<sub>2</sub>/NH<sub>3</sub>/NO<sub>x</sub> is beneficial to control secondary inorganic aerosols in PM<sub>2.5</sub>. In this study, the Weather Research and Forecasting model with Chemistry model (WRF-Chem) was applied to study the impact on the PM<sub>2.5</sub> and its secondary inorganic aerosols using the scenario simulation method in the Beijing–Tianjin–Hebei (BTH) region. The results showed that the BTH region is characterized by being NH<sub>3</sub>-rich and having a higher [NH<sub>4</sub><sup>+</sup>]/[SO<sub>4</sub><sup>2-</sup>] ratio in southern BTH, with a ratio of more than 6.0. Source contribution to PM<sub>2.5</sub> was highest in the 30%\_SO<sub>2</sub>\_40%\_NH<sub>3</sub>\_40%\_NO<sub>x</sub> scenario, with a contribution ratio of 6.8%, followed by 3.8% contribution in the 30%\_SO<sub>2</sub>\_40%\_NH<sub>3</sub> scenario, and a 3.4% contribution in the 30%\_SO<sub>2</sub>\_60%\_NH<sub>3</sub>\_60%\_NO<sub>x</sub> scenario. These results indicate that synergistic reduction measures may be suitable for controlling PM<sub>2.5</sub> concentrations. A lower sensitivity factor,  $\beta$  value between PM<sub>2.5</sub> and NH<sub>3</sub> suggests that solely reducing NH<sub>3</sub> emissions is not beneficial for the BTH region. However, this study indicates that the sensitivity of NO<sub>3</sub><sup>-</sup> would improve significantly if NH<sub>3</sub> emissions are reduced sharply. A slight reduction in NH<sub>3</sub> was found to be beneficial for controlling NO<sub>3</sub><sup>-</sup> in medium and small cities, while a significant decrease in NH<sub>3</sub> would be more suitable for mega-cities. The study also observed that SO<sub>4</sub><sup>2-</sup> and its constituents continued to decrease with a consistent  $\beta$  value of approximately 0.14 in the 30%\_SO<sub>2</sub>\_%\_NH<sub>3</sub> scenario and between 10.5 and 12.8 in the 30%\_SO<sub>2</sub>\_%\_NH<sub>3</sub>\_%\_NO<sub>x</sub> scenario. These findings suggest that a synergistic reduction in SO<sub>2</sub>-NH<sub>3</sub>-NO<sub>x</sub> emissions may be more effective in reducing PM<sub>2.5</sub> concentrations and its secondary inorganic aerosols (SIAs). However, it is important to ensure that the reduction in NH<sub>3</sub> and NO<sub>x</sub> exceeds 60% in low SO<sub>2</sub> concentration conditions.

**Keywords:** PM<sub>2.5</sub>; NH<sub>3</sub>; SIA; WRF-Chem; BTH



**Citation:** Wei, Z.; Mohamed Tahrin, N. Impact of Gaseous Pollutants Reduction on Fine Particulate Matter and Its Secondary Inorganic Aerosols in Beijing–Tianjin–Hebei Region. *Atmosphere* **2023**, *14*, 1027. <https://doi.org/10.3390/atmos14061027>

Academic Editor: Santtu Mikkonen

Received: 11 May 2023

Revised: 30 May 2023

Accepted: 8 June 2023

Published: 15 June 2023



**Copyright:** © 2023 by the authors. Licensee MDPI, Basel, Switzerland. This article is an open access article distributed under the terms and conditions of the Creative Commons Attribution (CC BY) license (<https://creativecommons.org/licenses/by/4.0/>).

## 1. Introduction

PM<sub>2.5</sub>, with an aerodynamic diameter of less than or equal to 2.5  $\mu\text{m}$ , is a significant component of atmospheric particulate matter. It has detrimental effects on human health, leading to an increased risk of respiratory diseases, as well as heart and brain conditions [1]. Additionally, atmospheric particulate matter plays a direct role in altering the scattering and absorption of light in the atmosphere and influences the formation of crystalline nuclei [2,3], thus impacting the climate [4–6]. In China, there are five major air pollution regions: the Beijing–Tianjin–Hebei region (BTH), the Pearl River Delta (PRD), the Yangtze River Delta (YRD), the Sichuan Basin Region (SBR), and the Fenwei Plain region (FPR) [7–11]. Among them, the BTH region stands out as the most polluted area in terms of fine particulate matter (PM<sub>2.5</sub> and PM<sub>10</sub>) pollution. Due to a severe pollution event in January 2013, the BTH region attracted significant public and media attention. This event was notable for its wide coverage, spanning 1.43 million square kilometers, as well as its prolonged duration

of nearly one month and the high levels of pollution it exhibited. It has been compared to historical atmospheric pollution events such as the London smog event and the Los Angeles photochemical smog event. Extensive research has confirmed that adverse weather conditions, elevated pollutant emissions, and the formation of secondary aerosols are the primary factors contributing to the formation of haze in this region [12–15]. Since then, China's air pollution control efforts have accelerated, leading to significant results in reducing air pollution. In the BTH region, there has been a significant decrease in PM<sub>2.5</sub> levels, with the annual average concentration dropping from  $108 \pm 34 \mu\text{g m}^{-3}$  in 2013 to  $55 \pm 13 \mu\text{g m}^{-3}$  in 2018, representing a nearly 50% decrease. This indicates the effectiveness and strength of PM<sub>2.5</sub> control measures implemented in the region. Furthermore, the annual average concentration of PM<sub>2.5</sub> in 337 cities in 2019 was  $36 \mu\text{g m}^{-3}$ , which is close to the national secondary air quality standard of  $35 \mu\text{g m}^{-3}$ . This demonstrates the progress made in reducing PM<sub>2.5</sub> pollution across the country and approaching the national air quality targets. Zhai et al. [16] discovered that the air quality has shown continuous improvement, with PM<sub>2.5</sub> reduction exceeding 30% in many cities. This positive trend can be attributed to the implementation of various air pollution control measures in China since 2013. The "Ten Air Pollution Measures" or the Action Plan for Air Pollution Prevention and Control have achieved significant progress, marking the initial success in the field of air pollution prevention and control. However, this is just the beginning of China's efforts in tackling air pollution. The country still has a long way to go to safeguard its Blue Sky and achieve the vision of a beautiful China by 2035.

However, despite the progress made in air pollution control, the issue of PM<sub>2.5</sub> pollution remains critical. The annual average PM<sub>2.5</sub> concentration continues to exceed the national secondary standard of  $35 \mu\text{g m}^{-3}$ . Moreover, the BTH region continues to experience heavy pollution events, with daily average concentrations reaching alarming levels, particularly during winter. This is primarily due to the sharp increase in particulate matter emissions associated with winter heating, overwhelming the self-cleaning capacity of the atmosphere. The presence of a winter inversion layer further hinders the dispersion and dilution of particulate matter, leading to the occurrence of severe haze pollution events. In addition to emissions, a significant portion of PM<sub>2.5</sub> is formed through atmospheric chemical reactions, a process known as new particle formation (NPF). This highlights the importance of understanding and addressing the underlying atmospheric chemistry processes that contribute to the production of PM<sub>2.5</sub>. Efforts to control PM<sub>2.5</sub> pollution and address its complex causes and sources remain crucial in the ongoing battle to improve air quality and achieve the goal of a cleaner and healthier environment. NPF is a widespread phenomenon that has been observed in various locations, as indicated by several studies [17–21]. Atmospheric chemistry processes play a significant role in the production of various compounds, including sulfates, nitrates, ammonium, and secondary organic aerosols. Within the realm of atmospheric chemistry research, there is a particular focus on studying the formation and characteristics of secondary inorganic aerosols [22–27]. Several studies [17,21,28] have specifically examined the reduction in SO<sub>2</sub> emissions. This is because SO<sub>2</sub> serves as a precursor for the formation of H<sub>2</sub>SO<sub>4</sub>, which plays a crucial role in the binary and ternary nucleation processes of NPF. By reducing SO<sub>2</sub> emissions, the concentration of sulfate and PM<sub>2.5</sub> can be effectively reduced. However, it is important to note that the reduction in SO<sub>2</sub> emissions can lead to an increase in the amount of free NH<sub>3</sub> in the atmosphere, resulting in an ammonia-rich environment. This shift in the chemical equilibrium has prompted recent research efforts to focus on the reduction in NH<sub>3</sub> emissions and propose corresponding control measures [29–32]. Chen et al. [33] conducted a study that confirmed the effectiveness of NH<sub>3</sub> reduction in inhibiting the production of secondary inorganic aerosols and controlling air pollution during the winter season in Baoding city. The reduction in NH<sub>3</sub> emissions has been identified as an effective and cost-efficient method for mitigating haze events, especially as the concentration of SO<sub>2</sub> continues to decrease [34]. Liu et al. [35] employed the Weather Research Forecasting and Chemistry model (WRF-Chem) to analyze the impact of NH<sub>3</sub> emission reduction on air quality. Their

findings demonstrated that a 15% reduction in SO<sub>2</sub> and NO<sub>x</sub> emissions resulted in a decrease in PM<sub>2.5</sub> concentration by 1–3 μg m<sup>-3</sup>, which corresponds to approximately 3% of the levels observed in 2015. These studies primarily focused on the sensitivity analysis of NH<sub>3</sub>'s impact on PM<sub>2.5</sub>. However, few studies have investigated the effects of different combinations of precursor reduction on secondary inorganic aerosols. Additionally, there is limited research on the influence of various emission reduction strategies on the spatial distribution of component concentrations. Therefore, further research is needed to explore the comprehensive impacts of different precursor reduction approaches and their effects on the distribution of pollutant concentrations, including secondary inorganic aerosols, to enhance our understanding of air pollution control strategies and their effectiveness.

This study utilizes the WRF-Chem model coupled with the Model for Simulating Aerosol Interactions and Chemistry (MOSAIC) module to address air pollution issues in the BTH region. The research objectives of this study are as follows: (1). Identify “ammonia control” areas within the BTH region and compare the effects of different control measures. The study aims to assess and compare the impacts of various ammonia control strategies on air pollution. (2). Quantify the source contributions of PM<sub>2.5</sub> and its secondary inorganic aerosols (such as SO<sub>4</sub><sup>2-</sup>, NH<sub>4</sub><sup>+</sup>, and NO<sub>3</sub><sup>-</sup>) through scenario simulations. The study aims to investigate the effects of NH<sub>3</sub> control on PM<sub>2.5</sub> and its secondary inorganic aerosols, particularly in conditions of low SO<sub>2</sub> concentration. (3). Analyze and quantify the influence of gas–particle partitioning based on different scenario simulations. The study aims to assess how different control measures affect the partitioning of pollutants between the gas and particle phases. By employing the WRF-Chem model with the MOSAIC module, this study aims to provide insights into the effectiveness of ammonia control measures, the source contributions of pollutants, and the impacts of gas–particle partitioning on air pollution in the BTH region. These findings can contribute to the development of targeted and effective strategies for air pollution control in the study area.

## 2. Methodology

### 2.1. Model Configurations and Simulation Design

The WRF-Chem model, developed by the United States' National Oceanic and Atmospheric Administration (NOAA)/Earth System Research Laboratories (ESRL), is a three-dimensional chemical transport model widely utilized for simulating regional air quality worldwide. This model is favored for its open-source nature and user-friendly features [36,37]. In conjunction with the WRF-Chem model, the WRF model, which is a meteorological model, was employed to generate meteorological fields that drive the WRF-Chem model. Prior to running the WRF model, it is necessary to utilize the *geogrid.exe* component of the pre-processing WPS system to extract terrain data within the designated domain. For our study, topography data from the United States Geological Survey (USGS) were employed, encompassing 23 soil classifications, to provide terrain and land-use data.

For our study, we employed WRF-Chem version 3.7 to simulate the winter period of January 2016, which represents the winter of one year. The simulations were conducted using two-layer nested domains. The first domain, referred to as Domain 1, covers East Asia with a grid resolution of 36 × 36 km as shown in Figure 1. The second domain, Domain 2, focuses on a specific area in northeastern China, encompassing Beijing, Tianjin, Hebei, Shandong, Henan, and Shanxi, with a grid resolution of 12 × 12 km. The BTH region, which is the primary area of interest, includes two municipalities, namely Beijing and Tianjin, along with eleven regional cities in Hebei province: Baoding, Cangzhou, Chengde, Handan, Hengshui, Qinhuangdao, Langfang, Shijiazhuang, Tangshan, Xingtai, and Zhangjiakou. Based on the size and population of these cities, we divided them into three categories: mega-cities (Beijing and Tianjin), medium cities (Baoding, Cangzhou, Handan, Qinhuangdao, Langfang, Shijiazhuang, Tangshan, and Xingtai), and small cities (Chengde, Hengshui, and Zhangjiakou). To ensure the accuracy of the simulations, we incorporated a spin-up period of 7 days to minimize the influence of initial conditions. In the first layer, we set the emissions outside Domain 1 to zero. The output from the first

layer was then used to provide initial and boundary fields for the second layer, which includes the BTH region. Additionally, to account for regional transport, Domain 2 was set to a broader area, not limited to the BTH region alone.

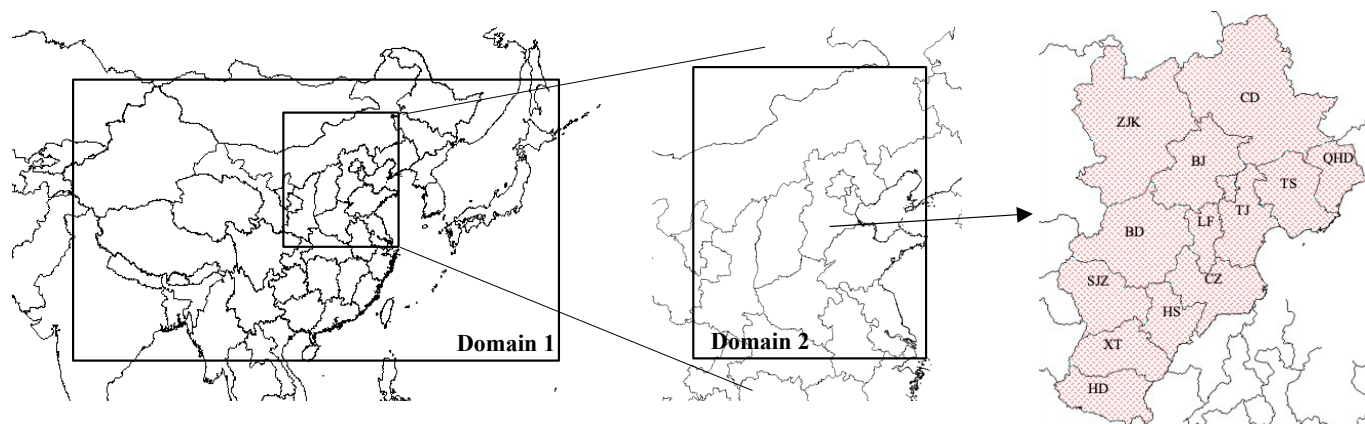


**Figure 1.** The simulated domain in WRF-Chem model and location of each city in the BTH region.

In our study, the WRF-Chem model incorporates various chemical schemes to capture the complex atmospheric chemistry. The gas-phase chemical reactions, photolysis, secondary generation of particulate matter, liquid-phase chemistry, and other calculation modules are included. For the gas-phase chemical mechanism, we selected the 1999 version of the Statewide Air Pollution Research Center (SAPRC-99) mechanism developed by Carter [38]. The SAPRC99 mechanism utilizes a lumped species approach, categorizing organic molecules based on their oxidation reactivity, emission magnitude, and internal bond types. It provides a comprehensive representation of various chemical reactions, including those involving isoprene, terpenes, ALDX, peroxy radicals, PAN analogues, isoprene products, organic acids, alkanes, acetone, ketones, and aromatic aldehydes. The aerosol module used in the WRF-Chem model is the Model for Simulating Aerosol Interactions and Chemistry (MOSAIC), which employs the Volatility Basis Set (VBS) with four volatility bins for the evolution of organic aerosols [39]. MOSAIC focuses on addressing gas–particle partitioning processes for various inorganic gases. It can be implemented using either the modal or sectional approach to represent the size distribution of aerosols. By incorporating SAPRC99 and MOSAIC, the WRF-Chem model allows us to simulate the intricate interactions between gases and aerosols, enabling a comprehensive analysis of atmospheric chemistry and the formation of secondary inorganic aerosols. WRF-Chem model with SAPRC-99 coupled with MOSAIC is able to calculate 34 aerosol components, including sulfate, nitrate, ammonium, organic carbon (OC), elemental carbon (EC), and others. These components are considered to exist in both externally mixed and internally mixed forms and can be removed from the atmosphere through dry and wet deposition processes. The SAPRC-99 mechanism combined with MOSAIC represents the most comprehensive version available in the model repository and is widely used for research purposes. It utilizes a sectional aerosol module and the VBS approach specifically for organic aerosols [37]. For photolysis rate calculation, we employed the Madronich Fast Troposphere Ultraviolet Visible (F-TUV) photolysis scheme. This scheme is not influenced by parameterized convection, ensuring accurate calculations of photolytic rates [40]. In terms of radiation processes, the Rapid Radiative Transfer Model for Global Climate Models (RRTMG) shortwave and long-wave radiation scheme is implemented in our model. This radiation scheme accounts for the direct effect of aerosols on radiation and is one of the primary processes associated with radiation calculations [41]. Morrison double-moment microphysics scheme is employed for the calculation of the indirect effect of aerosols [42]. This scheme can utilize both the modal and sectional approaches and is specifically designed to capture the interactions between aerosols and cloud microphysics. To accurately calculate the indirect effect, the aqueous phase chemistry is activated in the model. This allows

for the representation of aerosol–cloud interactions through cloud droplet activation and subsequent processes. As for the boundary layer scheme, we chose the Yonsei University scheme. This scheme incorporates an inverse gradient term to account for non-locally induced fluxes and considers entrainment processes at the top of the boundary layer. It provides a representation of boundary layer processes, which are crucial for capturing the vertical mixing and turbulent exchanges near the Earth’s surface. For land surface processes, we employed the Noah Land Surface Model. This model calculates heat and water vapor fluxes across land surfaces by considering various factors such as radiative forcing, cloud microphysical processes, precipitation forcing, land state variables, and land surface characteristics [43,44]. It helps simulate the interactions between the land surface and the atmosphere. For a comprehensive overview of the optimized configurations used in our study, see Table 1 or refer to the work of Wang et al. [45].

The emission inventory used in our model is based on the Multi-resolution Emission Inventory for China (MECI) developed by Tsinghua University for the year 2016. This inventory was evaluated and validated by Li et al. (2017) and Zheng et al. [46,47]. The MECI inventory provides emissions data for ten air pollutants including SO<sub>2</sub>, NO<sub>x</sub>, CO, NMVOC, NH<sub>3</sub>, BC, OC, PM<sub>10</sub>, PM<sub>2.5</sub>, and CO<sub>2</sub>. To obtain the input data for the WRF-Chem model, the MECI inventory is processed through spatial allocation, time allocation, and species allocation. The resulting data set has a resolution of 0.25° × 0.25° latitude and longitude and is used as the anthropogenic input data for the model. The VOC chemical mechanisms used in the model include CBIV, CB05, SAPRC99, SAPRC07, and RADM2. These mechanisms describe the oxidation and transformation processes of volatile organic compounds. The vertical resolution of the model is divided into 23 layers, with corresponding sigma levels ranging from 1.000 (near the ground) to 0.000 (top of the troposphere). This vertical division allows for a more accurate representation of atmospheric processes and interactions. The emissions of gases and aerosols from natural sources are estimated using the Model of Emissions of Gases and Aerosols from Nature (MEGAN) model [48,49]. MEGAN does take into account factors such as land cover, leaf area index, weather, and atmospheric chemical composition to estimate the emissions of VOCs, NO<sub>x</sub>, and CO from vegetation. By incorporating the MECI inventory for anthropogenic emissions and the MEGAN model for natural emissions, the complex interplay between human activities and natural sources in the simulation of air pollution can be captured.

**Table 1.** WRF-Chem model configurations and model set up used in this study.

Physical and Chemical Processes	Baseline Simulations
Simulation period	January 2016
Domain	East Asia (36 km), northern China (12 km)
Vertical resolution	23 layers from 1000 to 100 mb
Anthropogenic emissions	MEIC [ <a href="http://www.meicmodel.org/">http://www.meicmodel.org/</a> ; accessed on 25 April 2023]
Biogenic emissions	MEGAN 2 [48]
Dust emissions	GOCART dust emissions [50]
Sea-salt emissions	Gong [2003] [51]
Meteorological ICs and BCs	The National Centers for Environmental Prediction Final Analysis (NCEP-FNL) reanalysis data
Chemical IC and BC	Default for 36-km; nested down from the parent domain for 12-km
Gas-phase chemistry	SAPRC-99 [38]
Photolysis	Madronich F-TUV [40]
Aerosol module	4-bin MOSAIC aerosol with volatility basis set (VBS) [39,52]
Urban surface	Urban canopy model [53,54]
Shortwave radiation	RRTMG [41]
Longwave radiation	RRTMG [41]
Land surface	NOAH Land Surface Model [43,44]

Table 1. Cont.

Physical and Chemical Processes	Baseline Simulations
Surface layer	Monin–Obukhov [55,56]
PBL	Yonsei University Scheme (YSU) [57]
Cumulus	Grell 3D ensemble [58]
Microphysics	Morrison double-moment [42]

## 2.2. Scenarios Setting in Air Quality Model and Real-Time Monitoring Data

In this study, the month of January 2016 was selected for simulation to investigate the impact of reduced SO<sub>2</sub> emissions on PM<sub>2.5</sub> and its secondary inorganic aerosols. January was chosen because it represents a period of frequent heavy pollution weather, offering an opportunity to assess the effectiveness of emission reduction measures during severe pollution events in winter. Additionally, the SO<sub>2</sub> concentration in 2016 was relatively high, and a 70% reduction in emissions would align with the current air quality situation. By conducting simulations for January 2016, the study aimed to compare the characteristics of PM<sub>2.5</sub> pollution under high and low SO<sub>2</sub> concentrations and examine the influence of gaseous pollutants on PM<sub>2.5</sub> and its components. The findings of the study can provide valuable insights and reference for future emission reduction policies. To complement the modeling approach, the study also collected observational data on PM<sub>2.5</sub> and its components, including water-soluble organic carbon, nitrate, sulfate, OC, EC, and H<sup>+</sup>, as well as PM<sub>10</sub> and its components, in Handan city. In addition, gaseous pollutants including CO, CO<sub>2</sub>, NO, NO<sub>2</sub>, NO<sub>x</sub>, NO<sub>y</sub>, SO<sub>2</sub>, and meteorological parameters (including relative humidity, temperature, pressure, wind speed, wind direction, and rainfall) were measured at the same time. These measurements were obtained using a continuous dichotomous aerosol chemical speciation analyzer (Model ACSA-14; Kimoto Electric, Ltd., Osaka, Japan). The combination of model simulations and monitoring data enhances the comprehensiveness and accuracy of the study's analysis. Furthermore, data for the evaluation of the WRF-Chem model were obtained from the website of the China National Environmental Monitoring Center (CNEMC). This data source provides valuable information for assessing the performance and reliability of the model in capturing real-world atmospheric conditions and pollutant concentrations. By integrating model simulations, observational data, and external data sources, the study aims to provide a comprehensive understanding of the impact of reduced SO<sub>2</sub> emissions on PM<sub>2.5</sub> pollution and contribute to the development of effective air pollution control strategies. Additionally, the data used for the evaluation of the WRF-Chem model were obtained from the <http://www.cnemc.cn> (accessed on 25 April 2023).

The Brute-force method (BFM) is a sensitivity simulation approach used to determine the contribution of specific emission sources to PM<sub>2.5</sub> concentrations. It involves running the WRF-Chem model multiple times with different emission scenarios. The base case simulation considers all emission sources, while subsequent simulations turn off or modify specific sources to quantify their individual contributions to PM<sub>2.5</sub>. This method provides detailed insights into the impact of sources such as SO<sub>2</sub> and NH<sub>3</sub> on PM<sub>2.5</sub> and its components. Although it requires multiple runs and significant storage space, the BFM approach helps assess the effects of emission reductions on air quality and understand source contributions to PM<sub>2.5</sub> pollution.

The simulation period for the study spans from 25 December 2015 to 31 January 2016. A spin-up period of 7 days is included in the simulation to minimize the influence of initial conditions and allow the model to reach a more stable state. To reduce computational costs, the MOSAIC-4 bin aerosol module is selected, which represents aerosol size distribution using four different sized bins: 0.039–0.1 µm, 0.1–1 µm, 1–2.5 µm, and 2.5–10 µm. Table 2 provides details of the 11 different cases considered within a 12 km domain. The base case represents the scenario without any reduction in the emission inventory. The “30%\_SO<sub>2</sub>” case indicates a 70% reduction in SO<sub>2</sub> emissions, while “30%\_SO<sub>2</sub>\_80%\_NH<sub>3</sub>\_80%\_NO<sub>x</sub>”

corresponds to a scenario with a 30% reduction in SO<sub>2</sub> emissions and an 80% reduction in NH<sub>3</sub> and NO<sub>x</sub> emissions, compared to their original emission levels. The Air Pollution Index (API) was used as the primary indicator of air quality until 2013, with the main pollutants of the day determined by their highest concentrations. PM<sub>10</sub> and SO<sub>2</sub> were the dominant pollutants during that period. Over the years, the levels of SO<sub>2</sub> have been steadily decreasing in the region. In the BTH region, the average concentration of SO<sub>2</sub> dropped from approximately ~300 µg m<sup>-3</sup> in 2003 to 12 µg m<sup>-3</sup> in 2021, a reduction that took nearly 20 years. The annual average concentration of SO<sub>2</sub> in the BTH region declined from 41.7 µg m<sup>-3</sup> in 2016 to 12 µg m<sup>-3</sup> in 2021, representing a reduction of more than 70% (source: <https://www.mee.gov.cn>, accessed on 25 April 2023). Given the significant reduction in SO<sub>2</sub> levels, the study focuses on the “30%\_SO<sub>2</sub>” case, which represents a 70% reduction in SO<sub>2</sub> emissions. This case is chosen to investigate the source contribution of the SO<sub>2</sub> reduction in PM<sub>2.5</sub> levels.

**Table 2.** Summary of WRF-Chem model scenario setting in this study.

Case Name	Period	Description
Base		no emission reduction
30%_SO <sub>2</sub>		70% SO <sub>2</sub> emission reduction
80%_NH <sub>3</sub>		20% NH <sub>3</sub> emission reduction
60%_NH <sub>3</sub>		40% NH <sub>3</sub> emission reduction
40%_NH <sub>3</sub>		60% NH <sub>3</sub> emission reduction
30%_SO <sub>2</sub> _80%_NH <sub>3</sub>		70% SO <sub>2</sub> emission reduction and 20% NH <sub>3</sub> emission reduction
30%_SO <sub>2</sub> _60%_NH <sub>3</sub>		70% SO <sub>2</sub> emission reduction and 40% NH <sub>3</sub> emission reduction
30%_SO <sub>2</sub> _40%_NH <sub>3</sub>	25 December 2015–31 January 2016	70% SO <sub>2</sub> emission reduction and 60% NH <sub>3</sub> emission reduction
30%_SO <sub>2</sub> _80%_NH <sub>3</sub> _80%_NO <sub>x</sub>		70% SO <sub>2</sub> emission reduction, 20% NH <sub>3</sub> emission reduction, and 20% SO <sub>2</sub> emission reduction
30%_SO <sub>2</sub> _60%_NH <sub>3</sub> _60%_NO <sub>x</sub>		70% SO <sub>2</sub> emission reduction, 40% NH <sub>3</sub> emission reduction, and 40% SO <sub>2</sub> emission reduction
30%_SO <sub>2</sub> _40%_NH <sub>3</sub> _40%_NO <sub>x</sub>		70% SO <sub>2</sub> emission reduction, 60% NH <sub>3</sub> emission reduction, and 60% SO <sub>2</sub> emission reduction

### 3. Results

#### 3.1. Quality Assurance (QA) and Quality Control (QC) in 36 km and 12 km

##### 3.1.1. QA and QC in 36 km

Figure 2 illustrates the simulated results of CO, NO<sub>2</sub>, SO<sub>2</sub>, and PM<sub>2.5</sub> concentrations, along with their corresponding Mean Bias (MB) values, compared to urban monitoring data across China. The model results are first compared with the gridded emission inventory data obtained from <http://meicmodel.org.cn/> (accessed on 25 April 2023), showing a good spatial agreement with the emission data. The simulation results indicate higher pollutant concentrations in the central-eastern part of China, particularly in urban clusters, which aligns with the distribution of larger MB values. However, the Normal Mean Bias (NMB) values are generally within or lower than ±40%, as specified in Table 3 [59]. Notably, for CO, the WRF-Chem model captures the concentration levels well across the country, with an average NMB value of −3.4%. This suggests that the results from the first nest grid provide more accurate initial and boundary data for Domain 2. Regarding SO<sub>2</sub> and NO<sub>2</sub>, as atmospheric precursors, they are slightly underestimated over the domain, with simulated concentrations of 57.4 µg m<sup>-3</sup> and 32.9 µg m<sup>-3</sup>, respectively, compared to observed concentrations of 69.6 µg m<sup>-3</sup> and 54.7 µg m<sup>-3</sup>. Nevertheless, these underestimations fall within the criteria for satisfactory performance and are considered acceptable. However, it should be noted that some cities in the east-central region of China have overestimated

predictions relative to the reproduction of CO. The simulation results for PM<sub>2.5</sub> demonstrate better agreement compared to SO<sub>2</sub> and NO<sub>2</sub>. Most cities and regions show slight underestimations, as indicated by the MB image where they appear as small blue dots. However, in a few cities, especially large-scale urban agglomerations, the model tends to overestimate concentrations, like what was observed for SO<sub>2</sub> and NO<sub>2</sub>. Overall, the prediction of PM<sub>2.5</sub> is slightly underestimated, with an overall MB value of −11.1% and an NMB value of −12.4%.

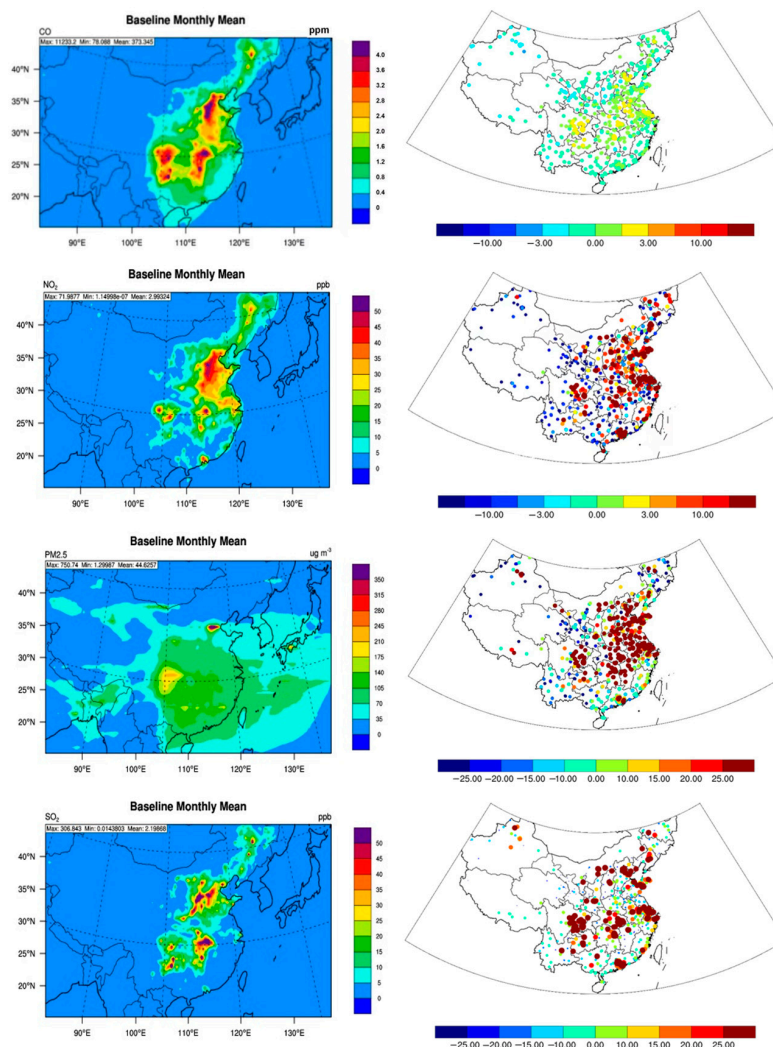


**Figure 2.** The simulated result of NO<sub>2</sub> (ppb), CO (ppm), SO<sub>2</sub> (ppb), and PM<sub>2.5</sub> ( $\mu\text{g m}^{-3}$ ) and their MB compared with observed concentration over 36 km domain.

In addition to evaluating pollutant concentrations, we also assessed the model's performance in simulating meteorological factors such as wind speed, wind direction, and temperature. Meteorological data are considered to provide a better reflection of the processes leading to peak pollution occurrences compared to pollutant concentrations such as PM<sub>2.5</sub>. For instance, the simulated wind speed showed good agreement with the observed data, with an average value of 2.9 m/s. The MB and NMB values for wind speed were 0.0% and 0.1%, respectively, over Domain 1. Overall, the meteorological data exhibited better consistency with the actual measurements compared to the simulated pollutant concentrations. The configuration of WRF-Chem in this study demonstrates its capability to simulate the processes of air pollution in China effectively. The output of WRF-Chem aligns with the published model verification criteria [60], indicating a satisfactory performance of the model in capturing important meteorological and pollution-related processes.

**Table 3.** Summary of WRF-Chem model evaluation in Domain 1.

	Obs	Model	MB	NMB	NME	RMSE
PCP24	17.4	3.0	−14.5	−83.0%	104.9%	44.1
PSFC	967.0	962.2	−4.8	−0.5%	1.6%	31.3
Q2	0.0	0.0	0.0	2.6%	15.9%	0.0
TEMP2	−6.4	−7.0	−0.6	−9.4%	−30.6%	2.7
WDIR10	214.0	209.0	−5.0	−2.4%	33.5%	120.1
WSPD10	2.9	2.9	0.0	0.1%	43.1%	1.7
CO	2.1	2.1	−0.1	−3.4%	102.7%	4.8
SO <sub>2</sub>	69.6	57.4	−12.2	−17.5%	121.8%	188.6
NO <sub>2</sub>	54.7	32.9	−21.8	−39.9%	77.1%	59.3
O <sub>3</sub>	27.6	26.6	−1.0	−3.6%	84.8%	29.3
PM <sub>10</sub>	141.8	81.4	−60.4	−42.6%	73.7%	163.2
PM <sub>2.5</sub>	89.6	78.5	−11.1	−12.4%	77.3%	133.8

MB: Mean bias; NMB: Normalized mean bias.

### 3.1.2. QA and QC in 12 km

In this study, the research focused on Domain 2, and we conducted verification and evaluation of the results within this domain to ensure the reliability of the WRF-Chem model. The corresponding statistical data can be found in Table 4, and Figure 3 presents a comparison between the observed and simulated concentrations of various pollutants in Domain 2, including NO<sub>2</sub>, CO, SO<sub>2</sub>, O<sub>3</sub>, PM<sub>10</sub>, and PM<sub>2.5</sub>. The NMB of PM<sub>2.5</sub> and NO<sub>2</sub> decreased from double-digit values to single-digit values, indicating an improvement in the model's performance. However, the prediction error of O<sub>3</sub> increased significantly, reaching −68.8% in Domain 2. It should be noted that the model's simulation of winter O<sub>3</sub> exhibits a considerable level of uncertainty, and further investigation is required to determine whether this is due to the model's processes or the unique characteristics of winter air pollution in northern China. Furthermore, Figure 4 shows the peculiar hourly concentration variation of O<sub>3</sub> in Handan city, with high concentrations exhibiting particularly high peaks during periods of lower photochemical reactions in winter. The presence of vertical transport processes for O<sub>3</sub>, which are not yet fully understood, may introduce additional uncertainty to the model results. Regarding PM<sub>2.5</sub>, the overestimation in the city is mainly concentrated at the three junctions in Hebei, Henan, and Shandong, as observed in Figure 3. However, this situation is not observed for PM<sub>10</sub>, where the monitoring and simulation values show extremely similar patterns. Overall, the results indicate that the model performs reasonably well for PM<sub>10</sub> but exhibits some limitations in simulating O<sub>3</sub> and PM<sub>2.5</sub>, particularly during winter and in specific regions. Further analysis and understanding of the underlying processes are necessary to improve the model's performance in these areas.

**Table 4.** Summary of WRF-Chem model evaluation in Domain 2.

	Obs	Model	MB	NMB	NME	RMSE
PCP24	17.4	3.1	−14.4	−82.5%	105.1%	44.1
PSFC	967.0	966.2	−0.8	−0.1%	1.0%	22.0
Q2	0.0	0.0	0.0	1.2%	14.9%	0.0
TEMP2	−6.4	−6.5	−0.1	−1.4%	−26.5%	2.3
WDIR10	214.0	207.2	−6.8	−3.2%	31.7%	116.2
WSPD10	2.9	3.0	0.0	0.9%	40.7%	1.6
CO	2.1	2.7	0.6	27.6%	84.7%	2.7
SO <sub>2</sub>	69.6	110.6	41.0	58.8%	117.2%	127.2
NO <sub>2</sub>	54.7	57.8	3.2	5.8%	59.8%	45.3
O <sub>3</sub>	27.6	8.6	−19.0	−68.8%	93.6%	33.9
PM <sub>10</sub>	141.8	100.0	−41.8	−29.5%	57.3%	120.9
PM <sub>2.5</sub>	89.6	97.4	7.8	8.7%	69.6%	91.3

NO<sub>2</sub> (ppb), CO (ppm), SO<sub>2</sub> (ppb), O<sub>3</sub> (ppb), PM<sub>10</sub> (μg m<sup>−3</sup>), and PM<sub>2.5</sub> (μg m<sup>−3</sup>).

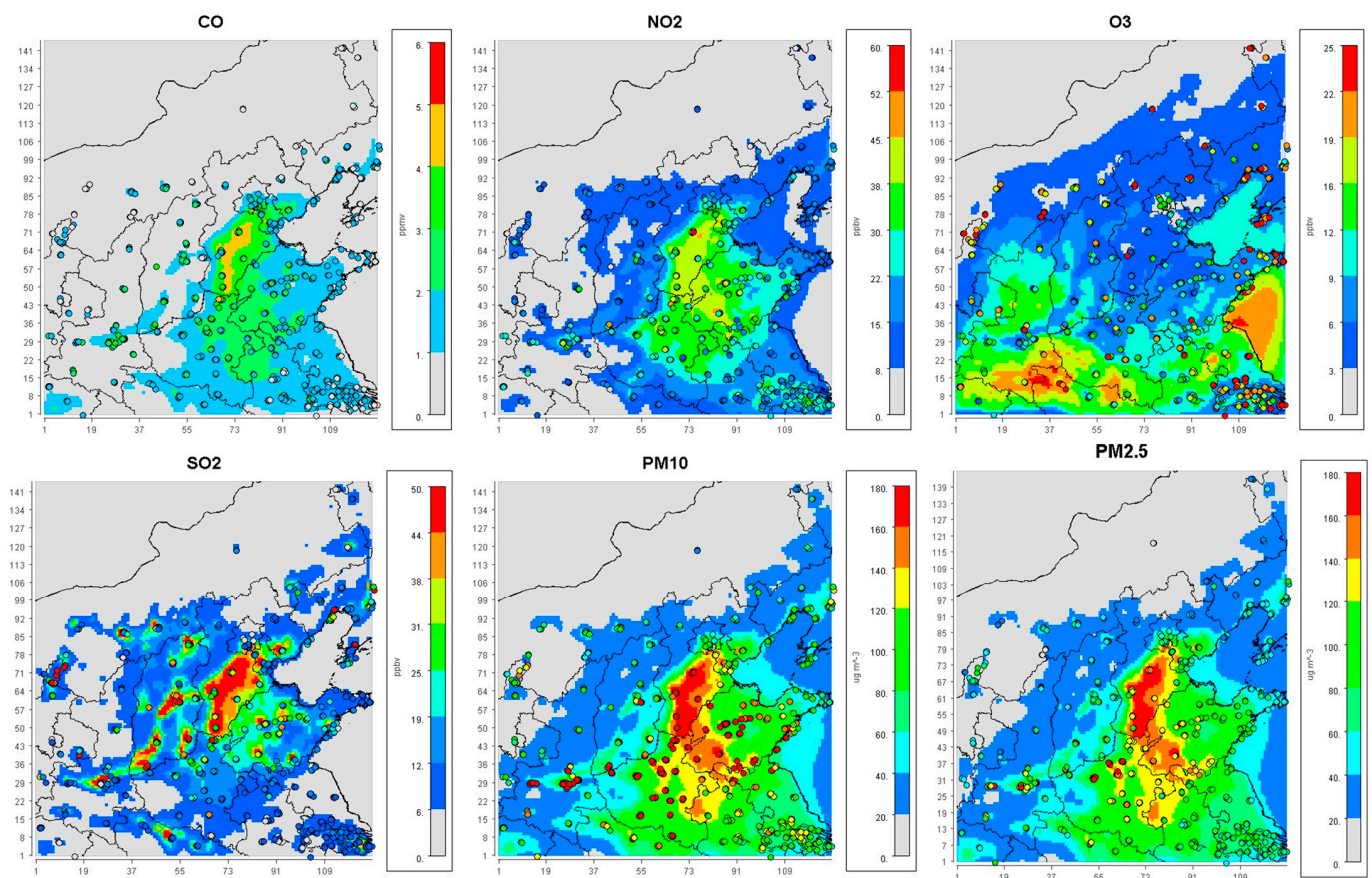


**Figure 3.** The simulated result of NO<sub>2</sub> (ppb), CO (ppm), SO<sub>2</sub> (ppb), O<sub>3</sub> (ppb), PM<sub>10</sub> ( $\mu\text{g m}^{-3}$ ), and PM<sub>2.5</sub> ( $\mu\text{g m}^{-3}$ ) and their monthly mean value over 12 km domain. The open circles indicate the monitoring sites.

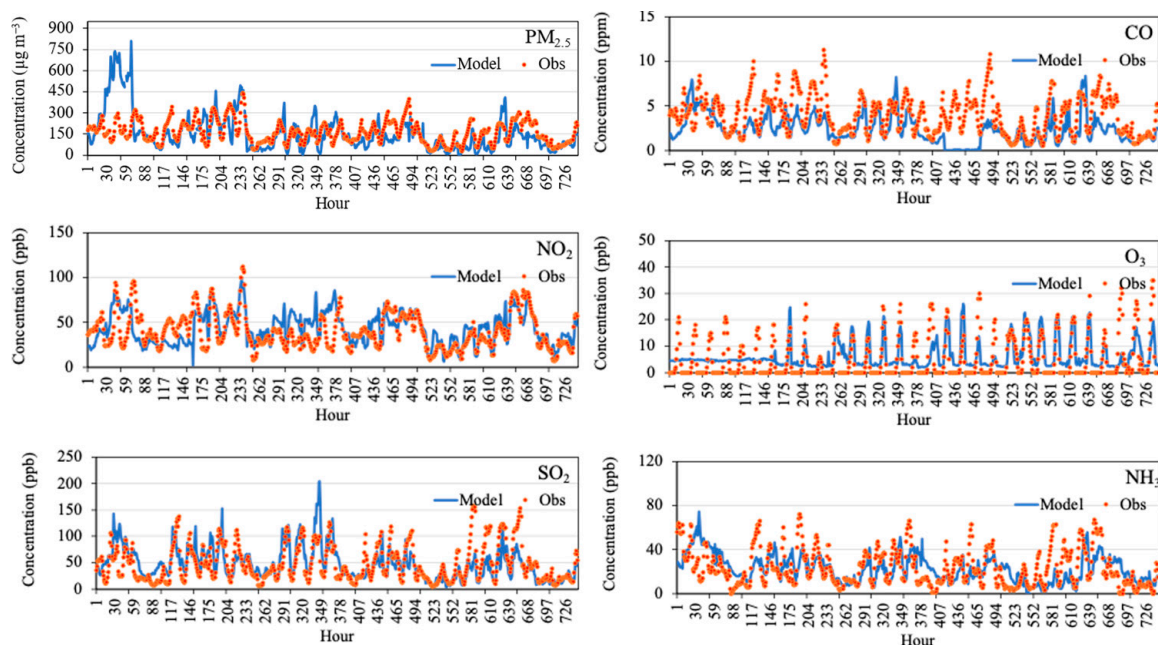


**Figure 4.** The hourly simulated and observed concentration of NO<sub>2</sub> (ppbv), CO (ppmv), SO<sub>2</sub> (ppbv), O<sub>3</sub> (ppbv), NH<sub>3</sub> (ppbv), and PM<sub>2.5</sub> ( $\mu\text{g m}^{-3}$ ) in Handan city in January 2016.

The simulation results for CO in Domain 2 were not as accurate as those in Domain 1, with a MB of  $0.6 \text{ mg m}^{-3}$  and a NMB of 27.6%. The southern Hebei region exhibited an overestimated concentration of CO, as indicated in Figure 3. This discrepancy may be attributed to the emission inventory of MEIC, which was generated using a bottom-up approach and could introduce a significant level of uncertainty, especially considering the active coal control measures implemented in Hebei province in January 2016 [46]. Similarly, the model tended to overestimate the concentration of SO<sub>2</sub>. The simulated concentration of SO<sub>2</sub> was 110.6 ppb, which was 1.59 times higher than the observed concentration. The NMB for SO<sub>2</sub> was 58.8%, indicating a high level of overestimation. It is worth noting that this study did not specifically discuss the impact of the overestimation of SO<sub>2</sub> on PM<sub>2.5</sub>. Overall, while the results mentioned above were acceptable for analyzing the correlation between changes in pollutant concentrations and PM<sub>2.5</sub> sensitivity analyses, there is room for improvement in accurately simulating CO and SO<sub>2</sub> concentrations in Domain 2. Further refinement of the emission inventory and model processes may help address these issues and enhance the overall performance of the simulation.

Figure 4 gave the hourly variation curves of NO<sub>2</sub> (ppb), CO (ppm), SO<sub>2</sub> (ppb), O<sub>3</sub> (ppb), NH<sub>3</sub> ( $\mu\text{g m}^{-3}$ ), and PM<sub>2.5</sub> ( $\mu\text{g m}^{-3}$ ) in Handan city located at the southernmost of Hebei province. For the six pollutants, it could be seen that the simulated results and the observed concentration present relatively good agreement, which meant that the model is not only credible in terms of monthly average values as above mentioned, but also confident in terms of high-resolution data. The biggest disparity could be seen in the simulation findings for O<sub>3</sub>, which was previously highlighted. This may require further work in the future. Additionally, we saw that several peaks of heavy pollution processes are not accurately replicated by the model, which was related to the model's own lack of mechanism, according to the simulation findings of PM<sub>2.5</sub> [15]. We have observed deviations in O<sub>3</sub>, NH<sub>3</sub>, SO<sub>2</sub>, and CO after 526 h, particularly in the case of O<sub>3</sub>. Regarding the primary pollutants, there are several factors contributing to these deviations. Firstly, we believe that the inventory data exhibit significant discrepancies due to the interpolation of sub-provincial data to each region, introducing errors in the process. Additionally, the model introduces larger deviations in pollutant simulations due to variations in meteorological conditions during the bias period. Furthermore, the monitoring data from Handan city are obtained from four monitoring stations, which may lead to sudden increases in monitoring values (such as SO<sub>2</sub>, CO, and ammonia) due to localized emissions occurring in a short period of time. Regarding O<sub>3</sub>, its deviations may be attributed to the nature of the model itself, as the model lacks the inclusion of the formation mechanism for O<sub>3</sub> in the winter.

### 3.2. Determination of NH<sub>3</sub>-Rich Region in BTH Region

Figure 5 provides insights into the characteristics of the ratio of  $[\text{NH}_4^+]/[\text{SO}_4^{2-}]$  across the Beijing–Tianjin–Hebei (BTH) region under different scenarios in January 2016. The results indicate that the BTH region experiences a high concentration of NH<sub>3</sub> during winter, leading to a high ratio of  $[\text{NH}_4^+]/[\text{SO}_4^{2-}]$  in the southern areas and a lower ratio in the northern areas. The region can be divided into four parts based on these ratios. The first part consists of Handan, Xingtai, Hengshui, and Cangzhou cities, where the NH<sub>3</sub>-rich condition is most prominent. The ratio of  $[\text{NH}_4^+]/[\text{SO}_4^{2-}]$  in these cities ranges from 6.0 to 7.5. The second part includes Shijiazhuang, Baoding, Langfang, and Tianjin cities, with a ratio between 4.5 and 6.0. These areas also exhibit a relatively high NH<sub>3</sub> concentration. The third part encompasses Beijing, Tangshan, and most areas of Qinhuangdao city, where the molar ratios range from 3.0 to 4.5. NH<sub>3</sub> levels in these areas are relatively lower compared to the previous parts. Finally, in most areas of northern Zhangjiakou and Chengde, the NH<sub>3</sub>-rich condition is the weakest, with molar ratios between 1.5 and 3.0. This may be attributed to lower levels of agricultural activities in these regions.

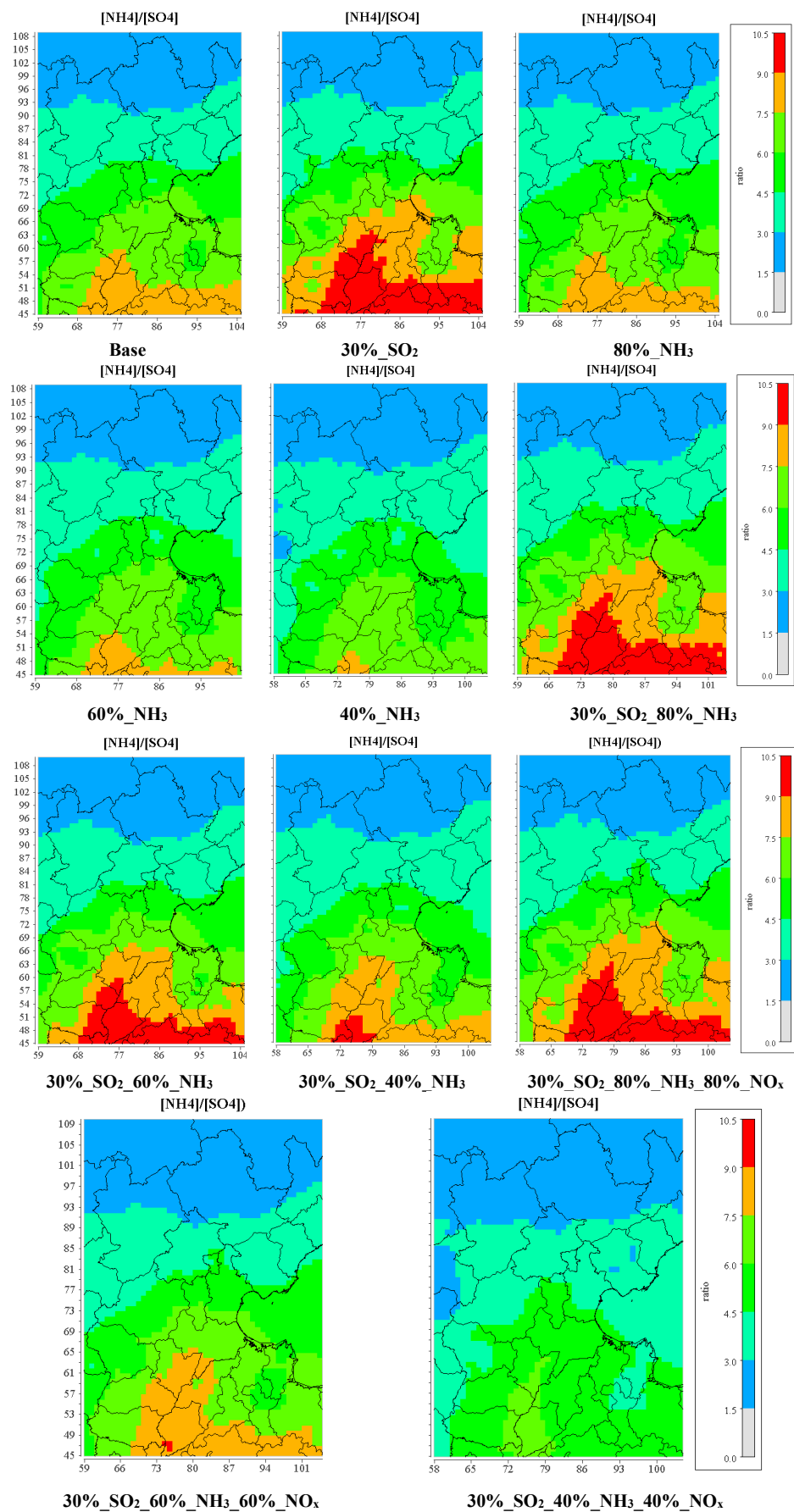


Figure 5. The distribution of  $[NH_4^+]/[SO_4^{2-}]$  using WRF-Chem model simulation in the BTH region.

When the emission of SO<sub>2</sub> is reduced by 70%, there is a significant increase in the ratio of [NH<sub>4</sub><sup>+</sup>]/[SO<sub>4</sub><sup>2-</sup>] in the southern part of the BTH region, particularly in the eastern areas of Handan, Xingtai, and Hengshui cities. The molar ratio in these regions exceeds 9.0. This increase in the ratio is attributed to the oxidation of SO<sub>2</sub> in the atmosphere, which forms H<sub>2</sub>SO<sub>4</sub>. The H<sub>2</sub>SO<sub>4</sub> then reacts with NH<sub>3</sub> to form (NH<sub>4</sub>)<sub>2</sub>SO<sub>4</sub> or NH<sub>4</sub>HSO<sub>4</sub>, leading to an increase in the concentration of NH<sub>4</sub><sup>+</sup> in the atmosphere. Henan and Shandong provinces are major contributors to NH<sub>3</sub> emissions [47]. High NH<sub>3</sub> emissions from the two provinces can be transported to other regions, potentially influencing the observed [NH<sub>4</sub><sup>+</sup>]/[SO<sub>4</sub><sup>2-</sup>] ratio. Interestingly, this study observed that the molar ratio remains relatively unchanged when comparing the 30%\_SO<sub>2</sub> scenario to the 30%\_SO<sub>2</sub>\_40%\_NH<sub>3</sub>\_40%\_NO<sub>x</sub> scenario in the third and fourth parts of the BTH region. This suggests that reducing NH<sub>3</sub> emissions alone does not significantly alter the characteristics of this region being rich in NH<sub>3</sub>. However, it was found that the orange color range (ratio between 7.5 and 9.0) gradually diminishes when NH<sub>3</sub> emissions are reduced alone, indicating a decrease in NH<sub>3</sub> concentration. Overall, these findings demonstrate the complex interactions between SO<sub>2</sub>, NH<sub>3</sub>, and other pollutants in the atmosphere. They highlight the importance of considering the impact of SO<sub>2</sub> emissions' reduction on NH<sub>3</sub> concentration and the ratio of [NH<sub>4</sub><sup>+</sup>]/[SO<sub>4</sub><sup>2-</sup>], taking into account regional emissions and transmission patterns.

In cases where the concentration of SO<sub>2</sub> is low (under 30%\_SO<sub>2</sub>), the high ratio region of [NH<sub>4</sub><sup>+</sup>]/[SO<sub>4</sub><sup>2-</sup>] tends to shrink when NH<sub>3</sub> emissions are continuously reduced or when both NH<sub>3</sub> and NO<sub>x</sub> emissions are reduced together. It was observed that the joint reduction in NH<sub>3</sub> and NO<sub>x</sub> leads to a greater shrinkage in the high ratio regions, particularly in the southern part of the BTH region, which includes Hebei province. Regardless of emission reduction efforts, the whole BTH region remains a high NH<sub>3</sub> region. However, this study highlights that the southern part of the BTH region, including Hebei province, is particularly sensitive to emission reductions. Reductions in SO<sub>2</sub> emissions lead to an increase in the ratio of [NH<sub>4</sub><sup>+</sup>]/[SO<sub>4</sub><sup>2-</sup>], while reductions in NH<sub>3</sub> or NH<sub>3</sub>\_NO<sub>x</sub> result in a decrease in the ratio of [NH<sub>4</sub><sup>+</sup>]/[SO<sub>4</sub><sup>2-</sup>]. Thus, the synergistic reduction in NH<sub>3</sub> and NO<sub>x</sub> is considered an effective approach for controlling the ratio of [NH<sub>4</sub><sup>+</sup>]/[SO<sub>4</sub><sup>2-</sup>] in the southern BTH region. It should be noted that in the northern part of the BTH region where the two mega-cities (Beijing and Tianjin) are located, the ratio of [NH<sub>4</sub><sup>+</sup>]/[SO<sub>4</sub><sup>2-</sup>] remains largely unchanged. This is attributed to relatively low SO<sub>2</sub> concentrations and minimal SO<sub>2</sub> emission reductions. The large number of motor vehicles in these cities may contribute to NH<sub>4</sub><sup>+</sup> production primarily through the conversion of local NO<sub>x</sub>, with little influence from regional transmission. However, further research is needed to fully understand this issue. Studying these differences in atmospheric chemical reactions between mega-cities and smaller cities can provide valuable insights. Overall, understanding the dynamics of the ratio of [NH<sub>4</sub><sup>+</sup>]/[SO<sub>4</sub><sup>2-</sup>] and the effects of emission reductions in different regions helps in designing effective strategies for air pollution control and management.

### 3.3. Source Contribution of PM<sub>2.5</sub> in Different Scenarios in BTH Region

This part discusses the contribution of various scenarios to PM<sub>2.5</sub> (particulate matter with a diameter of 2.5 μm or less) in different cities within the Beijing–Tianjin–Hebei (BTH) region. Table 5 shows that the 30%\_SO<sub>2</sub>\_40%\_NH<sub>3</sub>\_40%\_NO<sub>x</sub> scenario contributed an average of 6.8% to PM<sub>2.5</sub>, followed by 3.8% for 30%\_SO<sub>2</sub>\_40%\_NH<sub>3</sub>, and 3.4% for 30%\_SO<sub>2</sub>\_60%\_NH<sub>3</sub>\_60%\_NO<sub>x</sub>. Other scenarios had contributions below 3.0%. The contribution of PM<sub>2.5</sub> was generally very low in Beijing, with a reduction of only 2.2% in the 30%\_SO<sub>2</sub>\_40%\_NH<sub>3</sub>\_40%\_NO<sub>x</sub> scenario compared to 0.6% in the 30%\_SO<sub>2</sub> scenario. In Zhangjiakou, PM<sub>2.5</sub> showed a significant decline of 16.0% in the 30%\_SO<sub>2</sub>\_40%\_NH<sub>3</sub>\_40%\_NO<sub>x</sub> scenario, which was 12.3 times higher than the reduction observed in the 30%\_SO<sub>2</sub> scenario. Tianjin, like Beijing, is a mega-city where the contribution of PM<sub>2.5</sub> was also low. The smaller cities in the BTH region, such as Cangzhou, Handan, Xingtai, and Hengshui, were better suited to reducing multiple pollutants simultaneously. The average reduction in PM<sub>2.5</sub> in these smaller cities was approximately 2.5 times higher than in Beijing and

Tianjin. The overall impact of reducing individual pollutants on PM<sub>2.5</sub> concentration was minimal. However, when both SO<sub>2</sub> and NH<sub>3</sub> were reduced together, PM<sub>2.5</sub> exhibited a stronger decrease compared to reducing either pollutant alone. The combined reduction was not greater than the sum of the reductions achieved by individual pollutant reductions. To effectively control PM<sub>2.5</sub> concentration, the study suggests considering a synergistic reduction in SO<sub>2</sub>, NH<sub>3</sub>, and NO<sub>x</sub> emissions. These findings highlight the complex nature of PM<sub>2.5</sub> pollution and the need for comprehensive strategies involving multiple pollutants to effectively control and reduce PM<sub>2.5</sub> concentrations in the BTH region.

**Table 5.** Source contribution of emission reduction to PM<sub>2.5</sub> in the BTH region (units: %).

	Mega-City			Medium Cities						Small Cities			Mean	
	BJ	TJ	SJZ	BD	CZ	HD	LF	QHD	TS	XT	CD	HS		ZJK
30%_SO <sub>2</sub>	0.6	1.7	1.6	1.7	1.7	1.8	1.1	1.5	1.1	1.7	0.9	1.9	1.3	1.4
80%_NH <sub>3</sub>	−0.3	0.9	0.2	0.2	0.6	0.4	0.1	0.2	0.3	0.3	−0.1	0.5	−0.4	0.2
60%_NH <sub>3</sub>	−0.1	1.7	0.9	0.4	2.2	1.5	0.9	0.4	0.6	1.3	−0.1	1.9	0.0	0.9
40%_NH <sub>3</sub>	0.4	2.4	1.7	1.1	3.0	2.6	1.5	0.8	0.7	2.2	0.1	3.1	0.2	1.5
30%_SO <sub>2</sub> _80%_NH <sub>3</sub>	0.6	2.0	1.8	1.2	2.2	2.2	1.7	1.5	1.3	2.0	0.9	2.4	3.5	1.8
30%_SO <sub>2</sub> _60%_NH <sub>3</sub>	0.8	2.6	2.2	1.5	3.2	3.1	2.2	1.7	1.4	2.7	1.0	3.4	5.5	2.4
30%_SO <sub>2</sub> _40%_NH <sub>3</sub>	1.4	3.8	3.7	2.7	5.4	5.1	3.0	2.3	1.8	4.4	1.2	5.6	9.0	3.8
30%_SO <sub>2</sub> _80%_NH <sub>3</sub> _80%_NO <sub>x</sub>	0.6	1.7	1.5	1.2	2.1	2.1	1.5	1.9	1.2	1.8	1.4	2.1	4.4	1.8
30%_SO <sub>2</sub> _60%_NH <sub>3</sub> _60%_NO <sub>x</sub>	0.9	2.7	2.7	2.0	4.4	4.5	2.1	3.3	1.7	3.5	2.3	4.5	9.0	3.4
30%_SO <sub>2</sub> _40%_NH <sub>3</sub> _40%_NO <sub>x</sub>	2.2	5.3	5.5	4.6	9.3	9.8	4.7	6.3	3.4	7.9	4.0	9.8	16.0	6.8

Baoding: BD; Beijing: BJ; Cangzhou: CZ; Chengde: CD; Handan: HD; Hengshui: HS; Langfang: LF; Qinhuangdao: QHD; Shijiazhuang: SJZ; Tangshan: TS; Tianjin: TJ; Xingtai: XT; Zhangjiakou: ZJK.

To understand the sensitivity of PM<sub>2.5</sub> concentration to SO<sub>2</sub>, NH<sub>3</sub>, and NO<sub>x</sub>, the sensitivity factor (β) was used to study the sensitivity of PM<sub>2.5</sub> from those cases over BTH region [61,62]. The sensitivity factor can be defined as follows:

$$\frac{\Delta X}{X} = \beta * \frac{\Delta E}{E}$$

where  $\frac{\Delta X}{X}$  represents the relative changes in the PM<sub>2.5</sub> concentration and  $\frac{\Delta E}{E}$  denotes the relative change in NO<sub>x</sub> or NH<sub>3</sub> emissions. Figure 6 in the paper displays the sensitivity factor, β values for PM<sub>2.5</sub> concentration in response to reductions in SO<sub>2</sub> and NH<sub>3</sub> emissions. The β values for the 30%\_SO<sub>2</sub> scenario ranged from 0.3 to 5.1, which were higher compared to the β values for the %\_NH<sub>3</sub> scenario. This suggests that the PM<sub>2.5</sub> concentration is more sensitive to reductions in SO<sub>2</sub> emissions than to reductions in NH<sub>3</sub> emissions. The β values for mega-cities, such as Beijing and Tianjin, were lower than those for other cities in the 30%\_SO<sub>2</sub> scenario (also in the %\_NH<sub>3</sub> scenario). This difference in sensitivity could be attributed to the relocation of factories from Beijing and Tianjin, resulting in lower SO<sub>2</sub> emissions in these mega-cities. In contrast, Hebei province had higher SO<sub>2</sub> concentrations due to coal combustion, leading to higher β values [63]. The study found that PM<sub>2.5</sub> concentration is not highly sensitive to NH<sub>3</sub>, with a β value of less than 2. However, despite this lower sensitivity, the study discovered that a high reduction in NH<sub>3</sub> can still lead to a reduction in PM<sub>2.5</sub> by 1.5%. In the 30%\_80%\_NH<sub>3</sub> scenarios, the β value was significantly higher than that of the 30%\_SO<sub>2</sub> scenario, particularly in medium-sized cities. It is worth noting that the β value decreased with the reduction in NH<sub>3</sub>, which is an interesting finding. Additionally, the study observed that when both NH<sub>3</sub> and NO<sub>x</sub> emissions were reduced by 60% in the low 30%\_SO<sub>2</sub> scenario, the β values did not exhibit a linear increase but showed a particular sensitivity. This finding aligns with a previous study by Xu et al. [63]. In summary, the study suggests that future reduction policies should focus on strengthening the synergistic reduction in NH<sub>3</sub> and NO<sub>x</sub> emissions, particularly in conditions of low SO<sub>2</sub> concentrations. This approach could help achieve lower PM<sub>2.5</sub> concentrations.

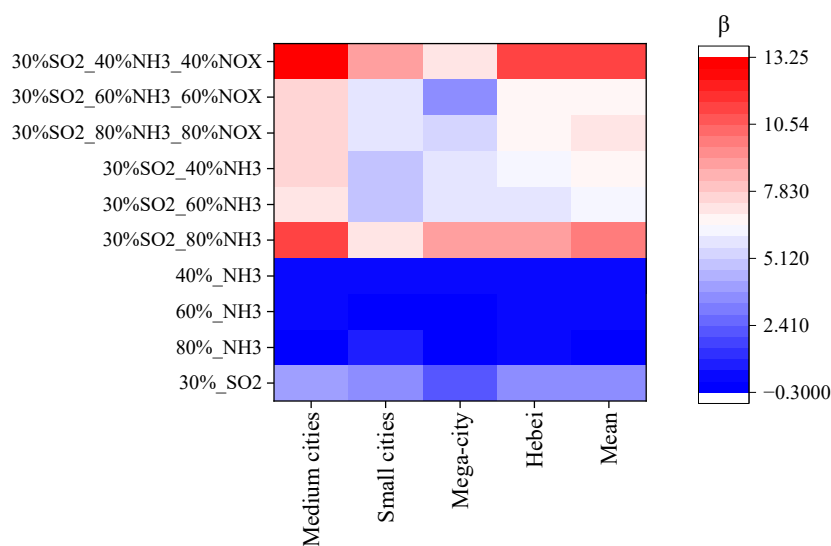


**Figure 6.** The sensitivity of gaseous pollution reduction to  $PM_{2.5}$  in different cities.

### 3.4. Impact of Gaseous Emission Reduction on Secondary Inorganic Aerosol in $PM_{2.5}$

#### 3.4.1. Impact of Emission Reduction in BTH Region on $NH_4^+$ , $SO_4^{2-}$ , and $NO_3^-$

Table 6 gives the proportions of secondary inorganic ions ( $NH_4^+$ ,  $SO_4^{2-}$ , and  $NO_3^-$ ) in  $PM_{2.5}$  under different scenarios. The study observed that the proportions of the three components ( $NH_4^+$ ,  $SO_4^{2-}$ , and  $NO_3^-$ ) in  $PM_{2.5}$  did not change significantly under different scenarios. Compared to the base scenario, there were rarely changes of more than 20% in these cases, with an average change ranging between 12.1% and 13.1%. Only in the 30%\_SO<sub>2</sub>\_40%\_NH<sub>3</sub>\_40%\_NO<sub>x</sub> scenario, significant decreases of 30.6%, 13.8%, and 39.7% were observed in the concentrations of  $NH_4^+$ ,  $SO_4^{2-}$ , and  $NO_3^-$ , respectively. The concentrations reached  $4.3 \mu g m^{-3}$ ,  $5.6 \mu g m^{-3}$ , and  $7.9 \mu g m^{-3}$ , respectively. In the 30%\_SO<sub>2</sub> scenario, the concentrations of  $NH_4^+$ ,  $SO_4^{2-}$ , and  $NO_3^-$  decreased by 16.1%, 20.0%, and 11.5%, respectively. The study found that reductions in SO<sub>2</sub> alone led to a reduction of more than 10% in  $NH_4^+$ ,  $SO_4^{2-}$ , and  $NO_3^-$  compared to their concentrations in 2016. NH<sub>3</sub> reduction had little effect on sulfate ( $SO_4^{2-}$ ) because the atmosphere already contained high levels of NH<sub>3</sub>. However,  $NH_4^+$  and  $NO_3^-$  decreased with NH<sub>3</sub> reduction. The study observed cases where higher pollutant concentrations were achieved with increased emission reduction [64,65]. This is due to the non-linear relationship between emission reduction and pollutant concentration. When NH<sub>3</sub> and NO<sub>x</sub> emissions were reduced together, the study found sustained decreases in the concentrations of  $NH_4^+$  and  $NO_3^-$ , ranging from 7.0% to 29.2% and from 0.6% to 38.7%, respectively. However, the concentration of  $SO_4^{2-}$  showed an opposite trend. These findings highlight the complex relationships between emission reductions and the concentrations of secondary inorganic ions in  $PM_{2.5}$ . Reductions in specific pollutants can have varying effects on the concentrations of different components, and non-linear relationships may exist.

#### 3.4.2. Sensitivity of Emission Reduction to $NH_4^+$ , $SO_4^{2-}$ , and $NO_3^-$ in Different Scenarios

To understand the impact of gaseous pollutants (SO<sub>2</sub>, NH<sub>3</sub>, and NO<sub>x</sub>) on secondary inorganic aerosols, the  $\beta$  values were calculated to evaluate their sensitivity. This study found that  $SO_4^{2-}$  exhibits higher sensitivity ( $\beta$ ) compared to  $NH_4^+$  and  $NO_3^-$ . The average  $\beta$  value for  $SO_4^{2-}$  was 0.27 in medium cities and 0.18 in mega-cities as shown in Figure 7. It is important to note that in mega-cities,  $NO_3^-$  showed no sensitivity to SO<sub>2</sub> reduction alone due to the suppression of  $NO_3^-$  production caused by decreased aerosol liquid water content [66]. When NH<sub>3</sub> reduction was implemented, high sensitivity was observed in  $NH_4^+$  and  $NO_3^-$ , particularly in  $NO_3^-$ . The  $\beta$  values for  $NH_4^+$  and  $NO_3^-$  in other cities were 0.30 and 0.41, respectively, which were 3.8 and 4.2 times higher than those in mega-cities. With an increase in NH<sub>3</sub> reduction (from 20% to 60%), the sensitivity of

SO<sub>4</sub><sup>2-</sup> weakened, as indicated by a decrease in the β value from 0.09 to 0.01 in all cities, which aligns with the conclusions of Cheng et al. [67]. The β values for NH<sub>4</sub><sup>+</sup> and NO<sub>3</sub><sup>-</sup> decreased from 0.30 and 0.41 to 0.12 and 0.17, respectively, in other cities. In contrast, in mega-cities, the β values for NH<sub>4</sub><sup>+</sup> and NO<sub>3</sub><sup>-</sup> increased from 0.08 to 0.09 (up to 0.10) and from 0.10 to 0.15 (up to 0.17), respectively. This suggests that a slight reduction in NH<sub>3</sub> is beneficial for controlling NO<sub>3</sub><sup>-</sup> in medium and small cities, while a more substantial decrease in NH<sub>3</sub> is more suitable for mega-cities.

Table 6. The proportion of secondary inorganic ions in PM<sub>2.5</sub> under setting scenarios.

Scenarios	NH <sub>4</sub> <sup>+</sup>	SO <sub>4</sub> <sup>2-</sup>	NO <sub>3</sub> <sup>-</sup>	NH <sub>4</sub> <sup>+</sup>	SO <sub>4</sub> <sup>2-</sup>	NO <sub>3</sub> <sup>-</sup>	NH <sub>4</sub> <sup>+</sup>	SO <sub>4</sub> <sup>2-</sup>	NO <sub>3</sub> <sup>-</sup>
	Concentration (μg m <sup>-3</sup> )			Proportion in PM <sub>2.5</sub> (%)			Decrease (%)		
base	6.2	6.5	13.1	4.5%	4.6%	9.4%			
30%_SO <sub>2</sub>	5.2	5.2	11.6	3.9%	3.8%	8.4%	16.1%	20.0%	11.5%
80%_NH <sub>3</sub>	5.6	6.2	11.5	4.0%	4.4%	8.1%	9.7%	4.6%	12.2%
60%_NH <sub>3</sub>	5.8	6.4	12.1	4.3%	4.6%	8.6%	6.5%	1.5%	7.6%
40%_NH <sub>3</sub>	5.7	6.4	11.3	4.0%	4.6%	8.1%	8.1%	1.5%	13.7%
30%SO <sub>2</sub> _80%NH <sub>3</sub>	5.7	5.3	13.0	4.1%	3.9%	9.3%	8.1%	18.5%	0.8%
30%SO <sub>2</sub> _60%NH <sub>3</sub>	5.5	5.3	12.3	4.0%	3.9%	8.9%	11.3%	18.5%	6.1%
30%SO <sub>2</sub> _40%NH <sub>3</sub>	5.1	5.3	11.0	3.8%	3.9%	7.9%	17.7%	18.5%	16.0%
30%SO <sub>2</sub> _80%NH <sub>3</sub> _80%NO <sub>x</sub>	5.8	5.4	13.0	4.1%	3.9%	9.4%	6.5%	16.9%	0.8%
30%SO <sub>2</sub> _60%NH <sub>3</sub> _60%NO <sub>x</sub>	5.4	5.4	11.5	3.9%	4.0%	8.3%	12.9%	16.9%	12.2%
30%SO <sub>2</sub> _40%NH <sub>3</sub> _40%NO <sub>x</sub>	4.3	5.6	7.9	3.1%	4.1%	5.8%	30.6%	13.8%	39.7%

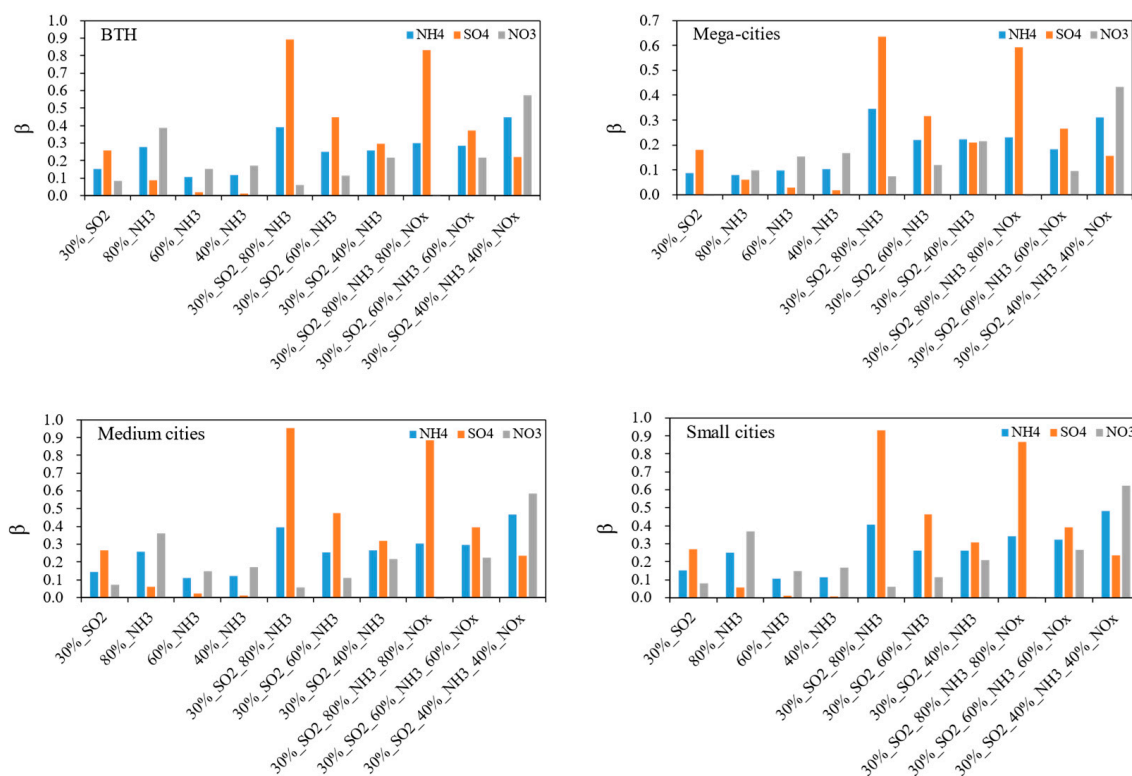


Figure 7. The sensitivity of gaseous pollution reduction to NH<sub>4</sub><sup>+</sup>, SO<sub>4</sub><sup>2-</sup>, and NH<sub>4</sub><sup>+</sup> in PM<sub>2.5</sub> in different cities.

In the 30%\_SO<sub>2</sub>\_80%\_NH<sub>3</sub> scenario, the sensitivity (β) of SO<sub>4</sub><sup>2-</sup> was much greater (β of 0.89) compared to NH<sub>4</sub><sup>+</sup> (β of 0.39) and NO<sub>3</sub><sup>-</sup> (β of 0.06) in the BTH region. The sensitivity of SO<sub>4</sub><sup>2-</sup> and NH<sub>4</sub><sup>+</sup> decreased significantly when transitioning from the 30%\_SO<sub>2</sub>\_80%\_NH<sub>3</sub> scenario to the 30%\_SO<sub>2</sub>\_40%\_NH<sub>3</sub> scenario, with β values decreasing to 0.30 and 0.26, respectively. However, the sensitivity of NO<sub>3</sub><sup>-</sup> continued to increase, with β values rising

from 0.06 in the 30%\_SO<sub>2</sub>\_80%\_NH<sub>3</sub> scenario to 0.11 in the 30%\_SO<sub>2</sub>\_60%\_NH<sub>3</sub> scenario, and further up to 0.22 in the 30%\_SO<sub>2</sub>\_40%\_NH<sub>3</sub> scenario. Until the 30%\_SO<sub>2</sub>\_40%\_NH<sub>3</sub> scenario, the study found that the  $\beta$  values of SO<sub>4</sub><sup>2-</sup>, NH<sub>4</sub><sup>+</sup>, and NO<sub>3</sub><sup>-</sup> were close to each other in all cities, indicating a similar sensitivity among these components. When reducing NH<sub>3</sub> and NO<sub>x</sub> together in the 30%\_SO<sub>2</sub> scenario, the sensitivity of SO<sub>4</sub><sup>2-</sup> decreased dramatically from the 30%\_SO<sub>2</sub>\_80%\_NH<sub>3</sub>\_80%\_NO<sub>x</sub> scenario to the 30%\_SO<sub>2</sub>\_40%\_NH<sub>3</sub>\_40%\_NO<sub>x</sub> scenario, with a decrease in  $\beta$  values from 0.83 to 0.22. In contrast, both NH<sub>4</sub><sup>+</sup> and NO<sub>3</sub><sup>-</sup> increased with greater emission reductions, particularly NO<sub>3</sub><sup>-</sup>, which exhibited the highest sensitivity ( $\beta$  value of 0.57) in the 30%\_SO<sub>2</sub>\_40%\_NH<sub>3</sub>\_40%\_NO<sub>x</sub> scenario, followed by NH<sub>4</sub><sup>+</sup> ( $\beta$  value of 0.45) and SO<sub>4</sub><sup>2-</sup> ( $\beta$  value of 0.22).

In conclusion, considering the issue that NO<sub>3</sub><sup>-</sup> has been the major component in PM<sub>2.5</sub> in some cities [62,68] a slight reduction in NH<sub>3</sub> emissions can be an effective approach to control NO<sub>3</sub><sup>-</sup> pollution in medium and small cities. This strategy can be relatively cost-effective and yield positive results. In mega-cities, a more significant reduction in NH<sub>3</sub> emissions may be necessary to effectively reduce NO<sub>3</sub><sup>-</sup> pollution. Mega-cities often face more complex pollution challenges, and addressing NO<sub>3</sub><sup>-</sup> pollution requires comprehensive strategies. The study suggests that the 30%\_SO<sub>2</sub>\_40%\_NH<sub>3</sub> scenario can yield good results for reducing the concentrations of SO<sub>4</sub><sup>2-</sup>, NH<sub>4</sub><sup>+</sup>, and NO<sub>3</sub><sup>-</sup>. This scenario balances the reduction in both SO<sub>2</sub> and NH<sub>3</sub> emissions, contributing to effective control of these three components. For cities specifically aiming to address NO<sub>3</sub><sup>-</sup> pollution, the study recommends adopting a synergistic reduction approach that includes controlling emissions of SO<sub>2</sub>, NH<sub>3</sub>, and NO<sub>x</sub>. The 30%\_SO<sub>2</sub>\_40%\_NH<sub>3</sub>\_40%\_NO<sub>x</sub> scenario is suggested as a better method for achieving this goal. The study also highlights that synergistic emission control (30%\_SO<sub>2</sub>\_40%\_NH<sub>3</sub>\_40%\_NO<sub>x</sub>) can be beneficial for simultaneously reducing concentrations of SO<sub>4</sub><sup>2-</sup> and NH<sub>4</sub><sup>+</sup>.

### 3.5. Impact of Emission Reduction in BTH Region on Size Distribution of Secondary Inorganic Aerosol

#### 3.5.1. Impact on Size Distribution of NH<sub>4</sub><sup>+</sup>, SO<sub>4</sub><sup>2-</sup>, and NH<sub>4</sub><sup>+</sup> in BTH Region

The averaged concentration of PM<sub>2.5</sub> in the base case was 122.5  $\mu\text{g m}^{-3}$ , with reductions ranging from 1.1% to 6.9% in different scenarios. Synergistic control measures led to more significant emission reductions. Most of the mass for the three substances (SO<sub>4</sub><sup>2-</sup>, NH<sub>4</sub><sup>+</sup>, and NO<sub>3</sub><sup>-</sup>) was found in bin2, accounting for 10.4% of PM<sub>2.5</sub>, followed by 2.8% in bin1 and 2.1% in bin3, as given in Table 7. When the concentration of SO<sub>2</sub> was reduced, there was a significant decrease in the three substances across the bins, with reductions of 17.9%, 15.7%, and 12.0%, respectively. The decrease in NH<sub>4</sub><sup>+</sup> was higher than that of SO<sub>4</sub><sup>2-</sup> and NO<sub>3</sub><sup>-</sup>. Under the 80%\_NH<sub>3</sub> scenario, the three substances showed a decrease of 3.5%, 10.0%, and 13.7% in bin1, bin2, and bin3, respectively. As NH<sub>3</sub> emission reductions continued to increase, bin1 for all three substances increased, possibly due to NH<sub>3</sub> affecting the gas–solid balance [39]. In the 40%\_NH<sub>3</sub> scenario, SO<sub>4</sub><sup>2-</sup> ions continued to increase, particularly in bin1 and bin2, deviating from the expected acid–base equilibrium. A similar trend was observed in the NH<sub>3</sub> scenario. Bin2 and bin3 of NO<sub>3</sub><sup>-</sup> showed a consistent decrease, indicating a clear linear relationship with NH<sub>3</sub>. Overall, while a significant reduction in NH<sub>3</sub> emissions slightly decreased the PM<sub>2.5</sub> concentration, it also led to changes in the distribution of SO<sub>4</sub><sup>2-</sup> and NH<sub>4</sub><sup>+</sup> ions, causing an increase in particle sizes in these categories instead of a decrease. This may impact their physical and chemical properties and hinder overall PM<sub>2.5</sub> control efforts [22,23] because the production of smaller particles may indicate that more NPF was produced in the atmosphere. Although there is no absolute increase in mass concentration, perhaps there is an increase in number concentration, which requires further experimental verification. NH<sub>3</sub> control may be more effective in controlling nitrate (NO<sub>3</sub><sup>-</sup>) concentration than sulfate (SO<sub>4</sub><sup>2-</sup>) in the future.

**Table 7.** Source contribution to secondary inorganic ions in BTH region (units:  $\mu\text{g m}^{-3}$ ).

	PM <sub>2.5</sub>	NH <sub>4</sub> <sup>+</sup>				SO <sub>4</sub> <sup>2-</sup>				NO <sub>3</sub> <sup>-</sup>			
		bin1	bin2	bin3	bin4	bin1	bin2	bin3	bin4	bin1	bin2	bin3	bin4
Base	122.5	1.1	4.3	0.8	0.0	0.8	4.5	1.2	0.1	2.6	8.9	1.6	0.1
30%_SO <sub>2</sub>	119.9	0.9	3.6	0.7	0.0	0.6	3.6	1.0	0.1	2.3	7.9	1.4	0.1
80%_NH <sub>3</sub>	121.2	1.1	3.8	0.7	0.0	0.8	4.3	1.1	0.1	2.5	7.7	1.3	0.0
60%_NH <sub>3</sub>	120.6	1.1	4.0	0.7	0.0	0.8	4.5	1.1	0.1	2.7	8.1	1.3	0.2
40%_NH <sub>3</sub>	119.6	1.1	3.9	0.7	0.0	0.8	4.5	1.1	0.1	2.6	7.6	1.1	0.2
30%_SO <sub>2</sub> _80%_NH <sub>3</sub>	120.1	1.0	3.9	0.8	0.0	0.6	3.7	1.0	0.1	2.6	8.8	1.6	0.1
30%_SO <sub>2</sub> _60%_NH <sub>3</sub>	119.2	1.0	3.8	0.7	0.0	0.6	3.7	1.0	0.1	2.7	8.2	1.4	0.1
30%_SO <sub>2</sub> _40%_NH <sub>3</sub>	117.2	1.0	3.5	0.6	0.0	0.6	3.7	1.0	0.1	2.7	7.2	1.1	0.2
30%_SO <sub>2</sub> _80%_NH <sub>3</sub> _80%_NO <sub>x</sub>	120.5	1.0	4.0	0.8	0.0	0.6	3.8	1.0	0.1	2.6	8.8	1.6	0.1
30%_SO <sub>2</sub> _60%_NH <sub>3</sub> _60%_NO <sub>x</sub>	118.7	1.0	3.7	0.7	0.0	0.6	3.8	1.0	0.1	2.5	7.7	1.3	0.1
30%_SO <sub>2</sub> _40%_NH <sub>3</sub> _40%_NO <sub>x</sub>	114.1	0.8	3.0	0.5	0.0	0.7	3.9	1.0	0.1	1.9	5.3	0.7	0.1

bin1: 0.039–0.1  $\mu\text{m}$ ; bin2: 0.1–1  $\mu\text{m}$ ; bin3: 1–2.5  $\mu\text{m}$ ; bin4: 2.5–10  $\mu\text{m}$ .

The reduction in each bin of SO<sub>4</sub><sup>2-</sup> remains unchanged when controlling both NH<sub>3</sub> and SO<sub>2</sub> simultaneously, as the emission of SO<sub>2</sub> remains unchanged. Therefore, the concentration of SO<sub>4</sub><sup>2-</sup> in each bin does not show significant variations. In contrast, the reduction in each bin of NH<sub>4</sub><sup>+</sup> continues to increase when both NH<sub>3</sub> and SO<sub>2</sub> are controlled together. However, when reducing NH<sub>3</sub> alone, the reduction in NH<sub>4</sub><sup>+</sup> was not as pronounced. The simultaneous control of NH<sub>3</sub> and SO<sub>2</sub> leads to more effective reductions in NH<sub>4</sub><sup>+</sup> in all bins. The behavior of NO<sub>3</sub><sup>-</sup> differs from the other two substances. The concentration in bin1 of NO<sub>3</sub><sup>-</sup> continues to increase, while bin2 and bin3 show a continuous decrease. Additionally, there is a significant increase in bin4. This suggests that more nitric acid is being absorbed by coarse particulate matter (PM<sub>2.5–10</sub>), despite weak nitric acid partial pressure [69]. This phenomenon may hinder the production of nitric acid in fine particulate matter [70].

As the concentrations of SO<sub>2</sub> and NH<sub>3</sub> decrease, both NO<sub>3</sub><sup>-</sup> and NH<sub>4</sub><sup>+</sup> show a continuous decrease in each bin. The reduction is particularly significant for NO<sub>3</sub><sup>-</sup>. The reduction in NO<sub>3</sub><sup>-</sup> can range from 0.4% to 40.4%, indicating a reduction in the mass concentration of NO<sub>3</sub><sup>-</sup> by approximately 40%. This reduction occurs simultaneously in all three bins. While the reduction in NH<sub>4</sub><sup>+</sup> is not as pronounced as that of NO<sub>3</sub><sup>-</sup>, it still shows a noticeable decrease. The mass concentration of NH<sub>4</sub><sup>+</sup> decreases by 7.0%, 13.9%, and 30.6% in the three scenarios, respectively. The reduction in NH<sub>4</sub><sup>+</sup> in the last scenario is 4.4 times that of the first scenario. The reduction in SO<sub>4</sub><sup>2-</sup> ions is relatively smaller compared to NO<sub>3</sub><sup>-</sup> and NH<sub>4</sub><sup>+</sup>. The decrease in SO<sub>4</sub><sup>2-</sup> slightly decreases from 18.0% to 16.3% and 15.2%. This reduction is mainly observed in bin1 and bin2.

### 3.5.2. Sensitivity of Emission Reduction to NH<sub>4</sub><sup>+</sup>, SO<sub>4</sub><sup>2-</sup>, and NH<sub>4</sub><sup>+</sup> in Different Cities

The  $\beta$  values in medium cities exhibit similar characteristics to those in small cities, with overall stronger sensitivity. The sensitivity order is as follows: medium cities > BTH region > small cities > mega-cities. When SO<sub>2</sub> emissions alone are reduced, the  $\beta$  values of NO<sub>3</sub><sup>-</sup> in bins 1 to 3 are negative as shown in Figure 8. This suggests that the concentration of NO<sub>3</sub><sup>-</sup> increases as SO<sub>4</sub><sup>2-</sup> decreases because the decrease in SO<sub>4</sub><sup>2-</sup> allows NH<sub>3</sub> to become available and react with HNO<sub>3</sub> in the atmosphere [71,72]. On the other hand, the  $\beta$  values of NH<sub>4</sub><sup>+</sup> and SO<sub>4</sub><sup>2-</sup> in bins 1 to 3 are positive. In the 30%\_SO<sub>2</sub> scenario, bin4 of both SO<sub>4</sub><sup>2-</sup> and NO<sub>3</sub><sup>-</sup> shows an increase. When NH<sub>3</sub> emissions are slightly reduced (80%\_NH<sub>3</sub>), bin1 of SO<sub>4</sub><sup>2-</sup> and NO<sub>3</sub><sup>-</sup> increases, while other bins decrease. Increasing the reduction in NH<sub>3</sub> emissions leads to higher  $\beta$  values in bins 2 and 3 of NO<sub>3</sub><sup>-</sup>, indicating that NH<sub>3</sub> emission reduction can effectively control NO<sub>3</sub><sup>-</sup> [62], particularly in mega-cities ( $\beta$  value of 0.21). The concentration of bins 3 and 4 in NH<sub>4</sub><sup>+</sup> decreases with NH<sub>3</sub> emission reduction in all cities. However, the  $\beta$  values decrease with increasing NH<sub>3</sub> emission reduction, resulting in a decrease in the concentration of bins 1 and 2 in SO<sub>4</sub><sup>2-</sup>. These findings suggest that

blindly and strongly reducing NH<sub>3</sub> may not effectively reduce NH<sub>4</sub><sup>+</sup> (PM<sub>2.5</sub>) but could contribute to an increase in SO<sub>4</sub><sup>2-</sup>.

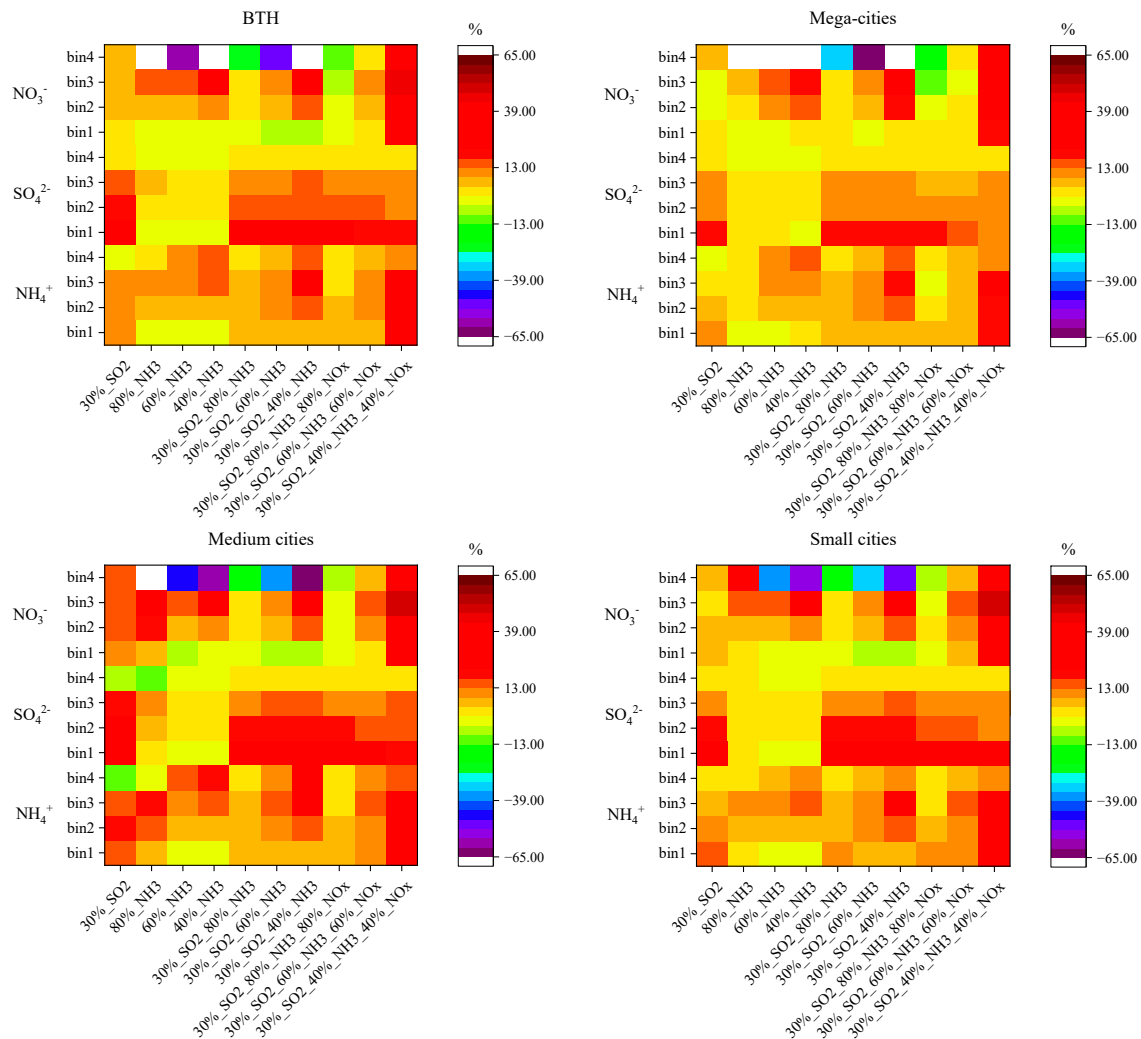


**Figure 8.** The sensitivity of gaseous pollutants to bins of NH<sub>4</sub><sup>+</sup>, SO<sub>4</sub><sup>2-</sup>, and NH<sub>4</sub><sup>+</sup> in different cities.

SO<sub>4</sub><sup>2-</sup> continuously decreases with increasing NH<sub>3</sub> abatement. Its sensitivity  $\beta$  value remains relatively constant in each bin, with mean values between 0.26–0.27, 0.16–0.17, 0.11–0.13, and 0.01–0.01 in BTH, respectively. This suggests that reducing NH<sub>3</sub> has a consistent and significant reduction effect on SO<sub>4</sub><sup>2-</sup>. Bin2, which is the main contributor to the mass of NH<sub>4</sub><sup>+</sup> and SO<sub>4</sub><sup>2-</sup>, shows a significant decrease in concentration. The  $\beta$  values for bin2 are between 0.08 and 0.17 for NH<sub>4</sub><sup>+</sup> and 0.02–0.17 for SO<sub>4</sub><sup>2-</sup>. This indicates that reducing NH<sub>3</sub> has a substantial reduction effect on both NH<sub>4</sub><sup>+</sup> and SO<sub>4</sub><sup>2-</sup> in bin2. When NH<sub>3</sub> and NO<sub>x</sub> are reduced simultaneously in low SO<sub>2</sub> emissions, there is little difference between mega-cities and small cities. In this scenario, the concentration of bins 1 to 4 in NO<sub>3</sub><sup>-</sup> increases significantly, with  $\beta$  values of –0.01, –0.01, –0.05, and –0.12 for bin1, bin2, bin3, and bin4, respectively. As the abatement efforts increase, the  $\beta$  values of NO<sub>3</sub><sup>-</sup> change from negative to positive and increase rapidly. For example, the  $\beta$  value of bin2 increases from –0.01 to 0.08 and then further increases to 0.34, indicating a rapid decrease in the concentration of NO<sub>3</sub><sup>-</sup>. Regarding NH<sub>4</sub><sup>+</sup>, the  $\beta$  value of bin2 increases from 0.06 to 0.11 and then further increases to 0.25. This suggests that higher abatement efforts for NH<sub>3</sub> and NO<sub>x</sub> may be beneficial for reducing the concentration of each bin for all three components (NH<sub>4</sub><sup>+</sup>, SO<sub>4</sub><sup>2-</sup>, and NO<sub>3</sub><sup>-</sup>).

#### 4. Discussion

The Beijing–Tianjin–Hebei region, which has been severely impacted by air pollution, witnessed a rapid decrease in PM<sub>2.5</sub> levels, and the reduction in alkaline gas NH<sub>3</sub> emissions has emerged as a crucial approach to further mitigate particulate matter pollution [29–31]. On one hand, NH<sub>3</sub> emissions are substantial, and thus far, we have not implemented effective measures to restrict them. Moreover, NH<sub>3</sub>, as an alkaline gas in the atmosphere, participates in various chemical reactions, forming a significant portion of secondary components in PM<sub>2.5</sub>. Based on the findings of Zhai et al. [72], a decrease in NH<sub>3</sub> emissions would lead to a decrease in particle nitrate levels by promoting more rapid deposition of total inorganic nitrate. Our findings suggest that a substantial reduction in NH<sub>3</sub> levels may lead to a corresponding decrease in NO<sub>3</sub><sup>−</sup> concentration. However, Xu et al. [62] argue that as SO<sub>2</sub> levels decrease, the responsiveness of PM<sub>2.5</sub> to the reduction in NH<sub>3</sub> also diminishes. This implies that measures aimed at mitigating PM<sub>2.5</sub> by reducing NH<sub>3</sub> must be approached with greater scientific precision. Cheng et al. [67] concluded that agricultural ammonia emission reduction accounted for 20.5–24.6% of PM<sub>2.5</sub> reduction during the 2015–2018 period, and this contribution is increasing. However, most studies focus on the positive impact of emission reduction on PM<sub>2.5</sub> and its secondary components [73,74]. Liu et al. [35] presented a negative perspective on the impact of reduction on acid rain, suggesting the need for different strategies based on regional variations. Consequently, more detailed reduction plans should be tailored to different regions. We contend that the level of detail in these reduction plans is appropriate, considering the distinct characteristics of each region. Instead, we put emphasize on NH<sub>3</sub> as a significant alkaline substance in the atmosphere, owing to its semi-volatile nature and involvement in atmospheric chemical reactions, which influence the formation of atmospheric particulate matter and gas–solid partitioning. These processes are closely linked to the formation, coalescence, condensation, and collision of PM<sub>2.5</sub> new particles. Furthermore, NH<sub>3</sub> reduction affects aerosol acidity, making it crucial to investigate the impact of NH<sub>3</sub> reduction on the distribution of secondary components. This research aims to investigate the distribution of secondary components in PM<sub>2.5</sub>, with a specific focus on examining the influence of NH<sub>3</sub> reduction. Additionally, it serves as a foundation for future studies on NH<sub>3</sub> reduction and its broader impacts on gas–solid partitioning.

#### 5. Conclusions

This study utilized the WRF-Chem model coupled with the MOSAIC module to examine the impact of gaseous pollutants (SO<sub>2</sub>, NH<sub>3</sub>, NO<sub>x</sub>) on PM<sub>2.5</sub> and its secondary inorganic aerosols in the Beijing–Tianjin–Hebei (BTH) region in January 2016. The findings revealed that the BTH region, particularly the southern part, experiences high levels of NH<sub>3</sub>. The molar ratio of [NH<sub>4</sub><sup>+</sup>]/[SO<sub>4</sub><sup>2−</sup>] in this area exceeds 6.0, with even higher values surpassing 9.0 in cities such as Handan, Xingtai, and Hengshui, particularly when reducing 70% of SO<sub>2</sub> emissions. The highest contribution to PM<sub>2.5</sub> was observed in the 30%\_SO<sub>2</sub>\_40%\_NH<sub>3</sub>\_40%\_NO<sub>x</sub> scenario, accounting for 6.8% of PM<sub>2.5</sub>, followed by 3.8% in the 30%\_SO<sub>2</sub>\_40%\_NH<sub>3</sub> scenario and 3.4% in the 30%\_SO<sub>2</sub>\_60%\_NH<sub>3</sub>\_60%\_NO<sub>x</sub> scenario. The reduction in gaseous pollutant emissions had a more significant impact on PM<sub>2.5</sub> levels in Hebei cities compared to mega-cities. For instance, in Zhangjiakou city, PM<sub>2.5</sub> concentrations decreased by 16.0% in the 30%\_SO<sub>2</sub>\_40%\_NH<sub>3</sub>\_40%\_NO<sub>x</sub> scenario, which was 7.3 times higher than the reduction observed in Beijing city. The study suggests that solely reducing NH<sub>3</sub> emissions may not effectively decrease PM<sub>2.5</sub> concentrations in the BTH region. Instead, a synergistic reduction in SO<sub>2</sub>, NH<sub>3</sub>, and NO<sub>x</sub> emissions is recommended for effectively lowering PM<sub>2.5</sub> levels. In settings with low SO<sub>2</sub> concentrations, it is crucial to ensure that NH<sub>3</sub> and NO<sub>x</sub> reductions reach a threshold of 60%. The study also observed that the β value of bin2 in NO<sub>3</sub><sup>−</sup> increased from −0.01 to 0.08 and then further to 0.34 when NH<sub>3</sub> and NO<sub>x</sub> emissions are reduced, highlighting the importance of synergistic emission reduction. Overall, the research provides valuable insights into the complex relationship between gaseous pollutants, PM<sub>2.5</sub>, and secondary aerosol components, emphasizing the

importance of considering multiple pollutants and specific scenarios for effective pollution mitigation policies.

**Author Contributions:** Z.W. was the data analyst and writer during the process of the thesis writing; N.M.T. served as the supervisor for the thesis writing. All authors have read and agreed to the published version of the manuscript.

**Funding:** We would like to thank Universiti Sains Malaysia, Short Term Grant 304/PFIZIK/6315382 for funding assistance.

**Institutional Review Board Statement:** Not applicable.

**Informed Consent Statement:** Not applicable.

**Data Availability Statement:** Data is unavailable due to privacy now. We will share data when appropriate.

**Conflicts of Interest:** The authors declare no conflict of interest.

## References

1. Donaldson, K.; Li, X.Y.; Macnee, W. Ultrafine (nanometre) particle mediated lung injury. *J. Aerosol Sci.* **1998**, *29*, 553–560. [[CrossRef](#)]
2. Tao, J.; Ho, K.F.; Chen, L.G.; Zhu, L.H.; Han, J.L.; Xu, Z.C. Effect of chemical composition of PM<sub>2.5</sub> on visibility in Guangzhou, China, 2007 spring. *Particuology* **2009**, *7*, 68–75. [[CrossRef](#)]
3. Pui, D.Y.H.; Chen, S.C.; Zuo, Z.L. PM<sub>2.5</sub> in China: Measurements, Sources, visibility and health effects, and mitigation. *Particuology* **2014**, *13*, 1–26. [[CrossRef](#)]
4. Pope, C.A., III; Burnett, R.T.; Thun, M.J.; Calle, E.E.; Krewski, D.; Ito, K.; Thurston, G.D. Lung cancer, cardiopulmonary mortality, and long-term exposure to fine particulate air pollution. *J. Am. Med. Assoc.* **2002**, *287*, 1132–1141. [[CrossRef](#)] [[PubMed](#)]
5. Maria, S.F.; Russell, L.M.; Gilles, M.K.; Myneni, S.C.B. Organic aerosol growth mechanism and their climate-forcing implications. *Science* **2004**, *306*, 1921–1924. [[CrossRef](#)]
6. Ramanathan, V.; Feng, Y. Air pollution, greenhouse gases and climate change: Global and regional perspectives. *Atmos. Environ.* **2009**, *43*, 37–50. [[CrossRef](#)]
7. Zhang, X.Y.; Wang, Y.Q.; Niu, T.; Zhang, X.C.; Gong, S.L.; Zhang, Y.M.; Sun, J.Y. Atmospheric aerosol compositions in China: Spatial/temporal variability, chemical signature, regional haze distribution and comparisons with global aerosols. *Atmos. Chem. Phys.* **2012**, *12*, 779–799. [[CrossRef](#)]
8. Cheng, Z.; Wang, S.X.; Jiang, J.K.; Fu, Q.Y.; Chen, C.H.; Xu, B.Y.; Yu, J.Q.; Hao, J.M. Longterm trend of haze pollution and impact of particulate matter in the Yangtze River Delta, China. *Environ. Pollut.* **2013**, *182*, 101–110. [[CrossRef](#)]
9. Tao, J.; Gao, J.; Zhang, L.; Zhang, R.; Che, H.; Zhang, Z.; Lin, Z.; Jing, J.; Cao, J.; Hsu, S.C. PM<sub>2.5</sub> pollution in a megacity of southwest China: Source apportionment and implication. *Atmos. Chem. Phys.* **2014**, *14*, 8679–8699. [[CrossRef](#)]
10. Tan, J.H.; Duan, J.C.; Zhen, N.J.; He, K.B.; Hao, J.M. Chemical characteristics and source of size-fractionated atmospheric particle in haze episode in Beijing. *Atmos. Res.* **2016**, *167*, 24–33. [[CrossRef](#)]
11. Tao, J.; Zhang, L.; Cao, J.; Zhang, R. A review of current knowledge concerning PM<sub>2.5</sub> chemical composition, aerosol optical properties and their relationships across China. *Atmos. Chem. Phys.* **2017**, *17*, 9485–9518. [[CrossRef](#)]
12. Wang, H.; Xu, J.Y.; Zhang, M.; Yang, Y.Q.; Shen, X.J.; Wang, Y.Q.; Chen, D.; Guo, J.P. A study of the meteorological causes of a prolonged and severe haze episode in January 2013 over central-eastern China. *Atmos. Environ.* **2014**, *98*, 146–157. [[CrossRef](#)]
13. Wang, L.T.; Wei, Z.; Yang, J.; Zhang, Y.; Zhang, F.F.; Su, J.; Meng, C.C.; Zhang, Q. The 2013 severe haze over southern Hebei, China: Model evaluation, source apportionment, and policy implications. *Atmos. Chem. Phys.* **2014**, *14*, 3151–3173. [[CrossRef](#)]
14. Wang, Y.S.; Yao, L.; Wang, L.L.; Liu, Z.R.; Ji, D.S.; Tang, G.Q.; Zhang, J.K.; Sun, Y.; Hu, B.; Xin, J.Y. Mechanism for the formation of the January 2013 heavy haze pollution episode over central and eastern China. *Sci. China Earth Sci.* **2014**, *57*, 14–25. [[CrossRef](#)]
15. Zheng, B.; Zhang, Q.; Zhang, Y.; He, K.B.; Wang, K.; Zheng, G.J.; Duan, F.K.; Ma, Y.L.; Kimoto, T. Heterogeneous chemistry: A mechanism missing in current models to explain secondary inorganic aerosol formation during the January 2013 haze episode in North China. *Atmos. Chem. Phys.* **2015**, *15*, 2031–2049. [[CrossRef](#)]
16. Zhai, S.X.; Jacob, D.J.; Wang, X.; Shen, L.; Li, K.; Zhang, Y.Z.; Gui, K.; Zhao, T.L.; Liao, H. Fine particulate matter (PM<sub>2.5</sub>) trends in China, 2013–2018: Separating contributions from anthropogenic emissions and meteorology. *Atmos. Chem. Phys.* **2019**, *19*, 11031–11041. [[CrossRef](#)]
17. Kulmala, M.; Laaksonen, A.; Pirjola, L. Parameterizations for sulfuric acid/water nucleation rates. *J. Geophys. Res. Atmos.* **1998**, *103*, 8301–8307. [[CrossRef](#)]
18. Korhonen, P.; Kulmala, M.; Laaksonen, A.; Viisanen, Y.; McGraw, R.; Seinfeld, J.H. Ternary nucleation of H<sub>2</sub>SO<sub>4</sub>, NH<sub>3</sub>, and H<sub>2</sub>O in the atmosphere. *J. Geophys. Res. Atmos.* **1999**, *104*, 26349–26353. [[CrossRef](#)]
19. Birmili, W.; Wiedensohler, A. New particle formation in the continental boundary layer: Meteorological and gas phase parameter influence. *Geophys. Res. Lett.* **2000**, *27*, 3325–3328. [[CrossRef](#)]

20. Kulmala, M.; Vehkamäki, H.; Petäjä, T.; Dal Maso, M.; Lauri, A.; Kerminen, V.M.; McMurry, P.H. Formation and growth rates of ultrafine atmospheric particles: A review of observations. *J. Aerosol Sci.* **2004**, *35*, 143–176. [[CrossRef](#)]
21. Boy, M.; Karl, T.; Turnipseed, A.; Mauldin, R.L.; Kosciuch, E.; Greenberg, J.; Rathbone, J.; Smith, J.; Held, A.; Barsanti, K.; et al. New particle formation in the Front Range of the Colorado Rocky Mountains. *Atmos. Chem. Phys.* **2008**, *8*, 1577–1590. [[CrossRef](#)]
22. Westerhoff, P.; Aiken, G.; Amy, G.; Debroux, J. Relationships between the structure of natural organic matter and its reactivity towards molecular ozone and hydroxyl radicals. *Water Res.* **1999**, *33*, 2265–2276. [[CrossRef](#)]
23. Mauldin, R.L., III; Berndt, T.; Sipilä, M.; Paasonen, P.; Petäjä, T.; Kim, S.; Kurtén, T.; Stratmann, F.; Kerminen, V.M.; Kulmala, M. A new atmospherically relevant oxidant of sulphur dioxide. *Nature* **2012**, *488*, 193–196. [[CrossRef](#)] [[PubMed](#)]
24. Chen, T.Z.; Chu, B.W.; Ge, Y.L.; Zhang, S.P.; Ma, Q.X.; He, H.; Li, S.M. Enhancement of aqueous sulfate formation by the coexistence of NO<sub>2</sub>/NH<sub>3</sub> under high ionic strengths in aerosol water. *Environ. Pollut.* **2019**, *252*, 236–244. [[CrossRef](#)]
25. Wang, S.Y.; Du, L.; Tsona, N.T.; Tsona, N.T.; Jiang, X.T.; You, B.; Xu, L.; Yang, Z.M.; Wang, W.X. Effect of NO<sub>x</sub> and SO<sub>2</sub> on the photooxidation of methylglyoxal: Implications in secondary aerosol formation. *J. Environ. Sci.* **2020**, *92*, 151–162. [[CrossRef](#)]
26. Sun, Y.H.; Chen, X.X.; Liu, L.; Xu, F.; Zhang, X.C. Mechanisms and Kinetics Studies of the Atmospheric Oxidation of Eugenol by Hydroxyl radicals and Ozone molecules. *Sci. Total Environ.* **2021**, *770*, 145203. [[CrossRef](#)]
27. Tian, M.; Liu, Y.; Yang, F.M.; Zhang, L.M.; Peng, C.; Chen, Y.; Shi, G.M.; Wang, H.B.; Luo, B.; Jiang, C.T.; et al. Increasing importance of nitrate formation for heavy aerosol pollution in two megacities in Sichuan Basin, southwest China. *Environ. Pollut.* **2019**, *250*, 898–905. [[CrossRef](#)]
28. Kulmala, M.; Pirjola, L.; Mäkelä, J.M. Stable sulphate clusters as a source of new atmospheric particles. *Nature* **2000**, *404*, 66–69. [[CrossRef](#)]
29. Pozzer, A.; Tsimpidi, A.P.; Karydis, V.A.; de Meij, A.; Lelieveld, J. Impact of agricultural emission reductions on fine-particulate matter and public health. *Atmos. Chem. Phys.* **2017**, *17*, 12813–12826. [[CrossRef](#)]
30. An, Z.S.; Huang, R.J.; Zhang, R.Y.; Tie, X.X.; Li, G.H.; Cao, J.J.; Zhou, W.J.; Shi, Z.G.; Han, Y.M.; Gu, Z.L.; et al. Severe haze in northern China: A synergy of anthropogenic emissions and atmospheric processes. *Proc. Natl. Acad. Sci. USA* **2019**, *116*, 8657–8666. [[CrossRef](#)]
31. Xu, Z.Y.; Liu, M.X.; Zhang, M.S.; Song, Y.; Wang, S.X.; Zhang, L.; Xu, T.T.; Wang, T.T.; Yan, C.Q.; Zhou, T.; et al. High efficiency of livestock ammonia emission controls in alleviating particulate nitrate during a severe winter haze episode in northern China. *Atmos. Chem. Phys.* **2019**, *19*, 5605–5613. [[CrossRef](#)]
32. Xu, J.; Chen, J.; Zhao, N.; Wang, G.C.; Yu, G.Y.; Li, H.; Huo, J.T.; Lin, Y.F.; Fu, Q.Y.; Guo, H.Y.; et al. Importance of gas-particle partitioning of ammonia in haze formation in the rural agricultural environment. *Atmos. Chem. Phys.* **2020**, *20*, 7259–7269. [[CrossRef](#)]
33. Chen, D.S.; Yang, N.; Zhou, Y.; Lang, J.L.; Wang, X.T. Impact of ammonia emission on the formation of the secondary inorganic aerosol in winter in a typical area in North China. *J. Saf. Environ.* **2017**, *17*, 1129–1135.
34. Pinder, R.W.; Adams, P.J.; Pandis, S.N. Ammonia emission controls as a cost-effective strategy for reducing atmospheric particulate matter in the eastern United States. *Environ. Sci. Technol.* **2007**, *41*, 380–386. [[CrossRef](#)] [[PubMed](#)]
35. Liu, M.; Huang, X.; Song, Y.; Tang, J.; Cao, J.J.; Zhang, X.Y.; Zhang, Q.; Wang, S.X.; Xu, T.T.; Kang, L.; et al. Ammonia emission control in China would mitigate haze pollution and nitrogen deposition, but worsen acid rain. *Proc. Natl. Acad. Sci. USA* **2019**, *116*, 7760–7765. [[CrossRef](#)]
36. Cai, C.J.; Zhang, X.; Wang, K.; Zhang, Y.; Wang, L.T.; Zhang, Q.; Duan, F.K.; He, K.B.; Yu, S.C. Incorporation of new particle formation and early growth treatments into WRF/Chem: Model improvement, evaluation, and impacts of anthropogenic aerosols over East Asia. *Atmos. Environ.* **2016**, *124*, 262–284. [[CrossRef](#)]
37. Wang, L.T.; Fu, J.S.; Wei, W.; Wei, Z.; Meng, C.C.; Ma, S.M.; Wang, J.D. How aerosol direct effects influence the source contributions to PM<sub>2.5</sub> concentrations over Southern Hebei, China in severe winter haze episodes. *Front. Environ. Sci. Eng.* **2018**, *12*, 1–13. [[CrossRef](#)]
38. Carter, W.P.L. *Implementation of the SAPRC99 Chemical Mechanism into the Models-3 Framework*; Report to the U.S. EPA; Statewide Air Pollution Research Center, University of California: Riverside, CA, USA, 2000.
39. Zaveri, R.A.; Easter, R.C.; Fast, J.D.; Peters, L.K. Model for simulating aerosol interactions and chemistry (MOSAIC). *J. Geophys. Res. Atmos.* **2008**, *113*, D13204. [[CrossRef](#)]
40. Madronich, S.S.; Flocke, S. The role of solar radiation in atmospheric chemistry. *Environ. Photochem.* **1999**, *2*, 1–26.
41. Iacono, M.J.; Delamere, J.S.; Mlawer, E.J.; Shephard, M.W.; Clough, S.A.; Collins, W.D. Radiative forcing by long-lived greenhouse gases: Calculations with the AER radiative transfer models. *J. Geophys. Res. Atmos.* **2008**, *113*, D13103. [[CrossRef](#)]
42. Morrison, H.; Thompson, G.; Tatarskii, V. Impact of cloud microphysics on the development of trailing stratiform precipitation in a simulated squall line: Comparison of one and two moment schemes. *Mon. Weather Rev.* **2009**, *137*, 991–1007. [[CrossRef](#)]
43. Chen, F.; Dudhia, J. Coupling an advanced land surface-hydrology model with the Penn State NCAR MM5 modeling system. Part I: Model implementation and sensitivity. *Mon. Weather Rev.* **2001**, *129*, 569–585. [[CrossRef](#)]
44. Ek, M.B.; Mitchell, K.B.; Lin, Y.; Rogers, B.; Grunmann, P.; Koren, V.; Gayno, G.; Tarpley, J.D. Implementation of Noah land surface model advances in the National Centers for Environmental Prediction operational mesoscale Eta model. *J. Geophys. Res.* **2003**, *108*, 8851. [[CrossRef](#)]

45. Wang, L.T.; Zhang, Y.; Wang, K.; Zheng, B.; Zhang, Q.; Wei, W. Application of Weather Research and Forecasting Model with Chemistry (WRF/Chem) over northern China: Sensitivity study, comparative evaluation, and policy implications. *Atmos. Environ.* **2016**, *124*, 337–350. [[CrossRef](#)]
46. Li, M.; Liu, H.; Geng, G.N.; Hong, C.P.; Liu, F.; Song, Y.; Tong, D.; Zheng, B.; Cui, H.Y.; Man, H.Y.; et al. Anthropogenic emission inventories in China: A review. *Natl. Sci. Rev.* **2017**, *4*, 834–866. [[CrossRef](#)]
47. Zheng, B.; Tong, D.; Li, M.; Liu, F.; Hong, C.P.; Geng, G.N.; Li, H.Y.; Li, X.; Peng, L.Q.; Qi, J.; et al. Trends in China's anthropogenic emissions since 2010 as the consequence of clean air actions. *Atmos. Chem. Phys.* **2018**, *18*, 14095–14111. [[CrossRef](#)]
48. Guenther, A.; Karl, T.; Harley, P.; Wiedinmyer, C.; Palmer, P.I.; Geron, C. Estimates of global terrestrial isoprene emissions using MEGAN (Model of Emissions of Gases and Aerosols from Nature). *Atmos. Chem. Phys.* **2006**, *6*, 3181–3210. [[CrossRef](#)]
49. Guenther, A.B.; Jiang, X.; Heald, C.L.; Sakulyanontvittaya, T.; Duhl, T.; Emmons, L.K.; Wang, X. The Model of Emissions of Gases and Aerosols from Nature version 2.1 (MEGAN2.1): An extended and updated framework for modeling biogenic emissions. *Geosci. Model Dev.* **2012**, *5*, 1471–1492. [[CrossRef](#)]
50. Ginoux, P.; Chin, M.; Tegen, I.; Prospero, J.M.; Holben, B.; Dubovik, O.; Lin, S.J. Sources and global distributions of dust aerosols simulated with the GOCART model. *J. Geophys. Res.* **2001**, *106*, 20255–20273. [[CrossRef](#)]
51. Gong, S.L. A parameterization of sea-salt aerosol source function for sub and super-micron particles. *Glob. Biogeochem. Cycles* **2003**, *17*, 1097. [[CrossRef](#)]
52. Shrivastava, M.; Fast, J.; Easter, R.; Gustafson, W.I., Jr.; Zaveri, R.A.; Jimenez, J.L.; Saide, P.; Hodzic, A. Modeling organic aerosols in a megacity: Comparison of simple and complex representations of the volatility basis set approach. *Atmos. Chem. Phys.* **2011**, *11*, 6639–6662. [[CrossRef](#)]
53. Kusaka, H.; Kimura, F. Thermal effects of urban canyon structure on the nocturnal heat island: Numerical experiment using a mesoscale model coupled with and urban canopy model. *J. Appl. Meteorol. Climatol.* **2004**, *43*, 1899–1910. [[CrossRef](#)]
54. Ikeda, R.; Kusaka, H. Proposing the simplification of the multilayer urban canopy model: Intercomparison study of four models. *J. Appl. Meteorol. Climatol.* **2010**, *49*, 902–919. [[CrossRef](#)]
55. Monin, A.S.; Obukhov, A.M. Basic laws of turbulent mixing in the surface layer of the atmosphere. *Contrib. Geo-Phys. Inst. Acad. Sci.* **1954**, *151*, 163–187. (In Russian)
56. Janić, Z.I. *Nonsingular Implementation of the Mellor-Yamada Level 2.5 Scheme in the NCEP Meso Model*; National Oceanic and Atmospheric Administration: Washington, DC, USA, 2001.
57. Hong, S.S.; Noh, Y.; Dudhia, J. A new vertical diffusion package with an explicit treatment of entrainment processes. *Mon. Weather Rev.* **2006**, *134*, 2318–2341. [[CrossRef](#)]
58. Grell, G.A.; Dévényi, D. A generalized approach to parameterizing convection combining ensemble and data assimilation techniques. *Geophys. Res. Lett.* **2002**, *29*, 1693. [[CrossRef](#)]
59. Zhang, Y.; Liu, P.; Pun, B.; Seigneur, C. A comprehensive performance evaluation of MM5-CMAQ for the Summer 1999 Southern Oxidants Study episode—Part I: Evaluation protocols, databases, and meteorological predictions. *Atmos. Environ.* **2006**, *40*, 4825–4838. [[CrossRef](#)]
60. Emery, C.; Liu, Z.; Russell, A.G.; Talat Odman, M.; Yarwood, G.; Kumar, N. Recommendations on statistics and benchmarks to assess photochemical model performance. *J. Air Waste Manag. Assoc.* **2017**, *67*, 582–598. [[CrossRef](#)] [[PubMed](#)]
61. Zhang, Q.Q.; Pan, Y.P.; He, Y.X.; Zhao, Y.H.; Zhu, L.Y.; Zhang, X.Y.; Xu, X.J.; Ji, D.S.; Gao, J.; Tian, S.L.; et al. Bias in ammonia emission inventory and implications on emission control of nitrogen oxides over North China Plain. *Atmos. Environ.* **2019**, *214*, 116869. [[CrossRef](#)]
62. Xu, G.Y.; Zhang, Q.Q.; Yao, Y.; Zhang, X.Y. Changes in PM<sub>2.5</sub> sensitivity to NO<sub>x</sub> and NH<sub>3</sub> emissions due to a large decrease in SO<sub>2</sub> emissions from 2013 to 2018. *Atmos. Ocean. Sci. Lett.* **2020**, *13*, 210–215. [[CrossRef](#)]
63. Wang, Y.; Xue, Y.F.; Tian, H.Z.; Gao, J.; Chen, Y.; Zhu, C.Y.; Liu, H.J.; Wang, K.; Hua, S.B.; Liu, S.H.; et al. Effectiveness of temporary control measures for lowering PM<sub>2.5</sub> pollution in Beijing and the implications. *Atmos. Environ.* **2017**, *157*, 75–83. [[CrossRef](#)]
64. Kwok RH, F.; Napelenok, S.L.; Baker, K.R. Implementation and evaluation of PM<sub>2.5</sub> source contribution analysis in a photochemical model. *Atmos. Environ.* **2013**, *80*, 398–407. [[CrossRef](#)]
65. Lu, D.B.; Mao, W.L.; Xiao, W.; Zhang, L. Non-linear response of PM<sub>2.5</sub> pollution to land use change in China. *Remote Sens.* **2021**, *13*, 1612. [[CrossRef](#)]
66. Stelson, A.W.; Seinfeld, J.H. Thermodynamic prediction of the water activity, NH<sub>4</sub>NO<sub>3</sub> dissociation constant, density and refractive index for the NH<sub>4</sub>NO<sub>3</sub>-(NH<sub>4</sub>)<sub>2</sub>SO<sub>4</sub>-H<sub>2</sub>O system at 25 °C. *Atmos. Environ.* (1967) **1982**, *16*, 2507–2514. [[CrossRef](#)]
67. Cheng, L.; Ye, Z.L.; Cheng, S.Y.; Guo, X.R. Agricultural ammonia emissions and its impact on PM<sub>2.5</sub> concentrations in the Beijing-Tianjin-Hebei region from 2000 to 2018. *Environ. Pollut.* **2021**, *291*, 118162. [[CrossRef](#)] [[PubMed](#)]
68. Lin, Y.C.; Zhang, Y.L.; Fan, M.Y.; Bao, M.Y. Heterogeneous formation of particulate nitrate under ammonium-rich regimes during the high-PM<sub>2.5</sub> events in Nanjing, China. *Atmos. Chem. Phys.* **2020**, *20*, 3999–4011. [[CrossRef](#)]
69. Wexler, A.S.; Seinfeld, J.H. Analysis of aerosol ammonium nitrate: Departures from equilibrium during SCAQS. *Atmospheric Environment. Part A Gen. Top.* **1992**, *26*, 579–591. [[CrossRef](#)]
70. Zhai, S.X.; Jacob, D.J.; Shah, V.; Yang, L.H.; Zhang, Q.; Sun, Y.L.; Wang, S.X.; Luo, G.; Yu, F.Q.; Woo, J.H.; et al. Coarse particulate matter air quality in East Asia: Implications for fine particulate nitrate. *Atmos. Chem. Phys.* **2023**, *23*, 4271–4281. [[CrossRef](#)]
71. Fu, X.; Wang, T.; Gao, J.; Wang, P.; Liu, Y.M.; Wang, S.X.; Zhao, B.; Xue, L.K. Persistent heavy winter nitrate pollution driven by increased photochemical oxidants in northern China. *Environ. Sci. Technol.* **2020**, *54*, 3881–3889. [[CrossRef](#)]

72. Zhai, S.X.; Jacob, D.J.; Wang, X.; Liu, Z.R.; Wen, T.X.; Shah, V.; Li, K.; Moch, J.M.; Bates, K.H.; Song, S.J.; et al. Control of particulate nitrate air pollution in China. *Nat. Geosci.* **2021**, *14*, 389–395. [[CrossRef](#)]
73. Ye, Z.L.; Guo, X.R.; Cheng, L.; Cheng, S.Y.; Chen, D.S.; Wang, W.L.; Liu, B. Reducing PM<sub>2.5</sub> and secondary inorganic aerosols by agricultural ammonia emission mitigation within the Beijing-Tianjin-Hebei region, China. *Atmos. Environ.* **2019**, *219*, 116989. [[CrossRef](#)]
74. Clappier, A.; Thunis, P.; Beekmann, M.; Putaud, J.P.; de Meij, A. Impact of SO<sub>x</sub>, NO<sub>x</sub> and NH<sub>3</sub> emission reductions on PM<sub>2.5</sub> concentrations across Europe: Hints for future measure development. *Environ. Int.* **2021**, *156*, 106699. [[CrossRef](#)] [[PubMed](#)]

**Disclaimer/Publisher's Note:** The statements, opinions and data contained in all publications are solely those of the individual author(s) and contributor(s) and not of MDPI and/or the editor(s). MDPI and/or the editor(s) disclaim responsibility for any injury to people or property resulting from any ideas, methods, instructions or products referred to in the content.